Coastal Engineering 183 (2023) 104315

Contents lists available at ScienceDirect

Coastal Engineering

journal homepage: www.elsevier.com/locate/coastaleng

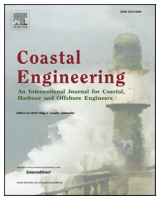

DualSPHysics modelling to analyse the response of Tetrapods against solitary wave

Jun Mitsui [a], Corrado Altomare [b], Alejandro J.C. Crespo [c,*], José M. Domínguez [c], Iván Martínez-Estévez [c], Tomohiro Suzuki [d], Shin-ichi Kubota [a], Moncho Gómez-Gesteira [c]

[a] Fudo Tetra Corporation, Japan
[b] Laboratori d'Enginyeria Marítima, Universitat Politecnica de Catalunya – BarcelonaTech, Spain
[c] Environmental Physics Laboratory, CIM-UVIGO, Universidade de Vigo, Spain
[d] Flanders Hydraulics Research, Belgium

ARTICLE INFO

Keywords:
SPH
DualSPHysics
Solitary wave
Tetrapods
Armour damage

ABSTRACT

The stability of Tetrapod armour units against solitary waves using Smoothed Particle Hydrodynamics (SPH) method is analysed in this work. To this purpose, the SPH-based DualSPHysics code was coupled with the multiphysics library Project Chrono. Tetrapod units are placed above a submerged mound. DualSPHysics solves the fluid-solid interaction, while Project Chrono solves the Tetrapod-mound interactions based on the contact and material properties of the block surface. The motion of the units during the simulation was compared with the physical model experiments where Tetrapods are made of mortar, and the mound is in PVC. The numerical results expressed as displacements of Tetrapods and damage ratio under different solitary waves are in reasonable agreement with the experiments, proving the capability of the DualSPHysics code to simulate challenging environments under the same numerical framework. The validated tool is then applied to study the stability for different coefficients of friction between mound and Tetrapods aiming at simulating the effects of different materials and surface roughness.

1. Introduction

During the Great East Japan Earthquake in 2011, many armour units installed at the breakwaters were scattered due to the generated tsunami waves (Esteban et al., 2014). These kind of events prompt reserachers to study in detail the effectiveness, resisistence and resilience of armour units and deatched breakwater for coastal risk mitigation. Hanzawa et al. (2012) investigated the stability of the blocks against solitary wave by hydraulic model experiments for breakwaters composed of wave-dissipating concrete blocks. Maruyama et al. (2014) and Mitsui et al. (2016) conducted hydraulic model experiments and numerical analyses to investigate the stability of armour units behind composite breakwaters against overflowing tsunami. These numerical studies are based on the hydrodynamic forces acting on the fixed individual units, and there is little study that directly calculates the behaviour of the units. Thus, predicting the stability of armour units due to tsunami by numerical simulation is an important but challenging task.

The behaviour of a coastal structure can be defined by a number of parameters, related to its hydrodynamic and structural response to the action of sea waves and currents. For a rubble mound breakwaters, the number of displaced armour units defines the damage ratio and expresses its structural stability. The hydraulic instability of the armour layer, usually referred and compared to the "undamaged" section, depends on hydrodynamic conditions and structural features, being expressed by parameters such as the incident wave height, the nominal diameter of the armour unit, the armour layer slope, the structural permeability etc. (Campos et al., 2020). Packing and interlocking of armour units might have a significant impact on the damage ratio and vary largely based on the armour unit shape. To this extent, studying the hydrodynamic behaviour of armour units under extreme wave conditions is fundamental for coastal engineering design.

The Tetrapod, which is the subject of this study, is a typical armour unit that has been widely used around the world since they were first employed in 1950. The shape of the Tetrapod is the result of testing a number of shapes in terms of hydraulic properties (including stability, wave overtopping reduction, and reflection reduction), construction properties (ease of fabrication and installation), and cost (Danel and Greslou, 1962). Although the shape is simple with four legs, when they

* Corresponding author.
E-mail address: alexbexe@uvigo.es (A.J.C. Crespo).

https://doi.org/10.1016/j.coastaleng.2023.104315
Received 1 December 2022; Received in revised form 14 March 2023; Accepted 9 April 2023
Available online 13 April 2023

are placed in combination, complex voids are formed between the units, which effectively dissipate wave energy. At the same time, the interlocking with adjacent units provides extra stability to wave action.

In the design of armour units, the required mass (or nominal diameter) of the unit is calculated to maintain stability against design waves and currents. There are various calculation formulae that have been proposed, such as the simple and widely used Hudson formula (Hudson, 1959), the formula by Van der Meer (1988) for armour units covering rubble mound breakwaters, and the formula proposed by Hanzawa et al. (1996) for wave-dissipating blocks installed in horizontally composite breakwaters. The range of application is limited to the range of tested conditions and structural layouts for which have been derived. In order to characterise the hydrodynamic behaviour of specific armour units, physical model tests are still carried out worldwide trying to cover the gaps of existing formulas from literature and going beyond the state-of-the-art. The research presented in Sande et al. (2018) analysed the stability of breakwater roundheads protected with Cubipod units. The authors compared single-layer armours with double-layer armours confirming that under certain conditions, the single-layer ones lead to the same behaviour. Safari et al. (2018) analysed the hydraulic stability of Starbloc armour unit and their effects on overtopping performance. Mares-Nasarre et al. (2022) performed physical model tests to study the stability of Cube-armored mound breakwaters in depth-limited breaking wave conditions, showing that lower stability was performed with respect to formulas from literature. Looking at improving the breakwater stability while reducing costs and materials, Yuksel et al. (2022) studied the performance of high-density cubes in the armor layers. The aforementioned studies are only a few examples of experimental modelling employed to characterise armour unit hydraulic behaviour. On the other hand, in recent years, it has become possible to predict the behaviour of individual armour units by directly evaluating the hydrodynamic forces acting on them and the resistance forces due to interlocking using numerical models (Dentale et al., 2018; Sarfaraz and Pak, 2018). Once such a method is established, it is expected to significantly reduce the cost and labour of conducting physical experiments. In addition, numerical analysis can be useful for clarifying phenomena by measuring hydraulic quantities at multiple locations and conducting parametric studies, which are difficult to do with physical experiments. Therefore, the authors aim to develop a numerical model that can reproduce the complex flow field around armour units and interlocking between units, and directly predict the stability against waves and currents.

The CFD (Computational Fluid Dynamics) models can be classified, according to their spatial derivation, into mesh-based or meshless models. Mesh-based methods are ideal for solving problems where the boundaries remain fixed and, in the presence of a free surface, with no large deformations of that surface. Yet, the domain can become highly distorted when simulating floating or moving objects, which can cause large mesh deformation. The latest developments, such as overset grids or embedded meshes in OpenFOAM (Chandar, 2019), can palliate those limitations, however simulating numerous fluid-driven objects that can collide with each other under wave action of waves remains a major challenge for mesh-based methods (Windt et al., 2020).

Mesh-based methods have been applied to study the interaction of sea waves and breakwaters, however they are rather focused on the analysis of pressure distribution in the filter layer and core of the breakwater and effects of the mound permeability on wave reflection and transmission (Koley et al., 2020; Celli et al., 2021), or on forces and pressures exerted on the crown wall and single armour units in order to determine indirectly possible failure mechanism, but without simulating them (Güler et al., 2018). In all these studies, however, the displacement and interaction of armour units and the damage evolution are not modelled.

Recently, meshless methods have grown in popularity as they can be applied to highly non-linear problems including moving complex geometries. For example, Gotoh et al. (2010) developed a coupled model of the MPS and Discrete Element Method (DEM) to analyse the movement of armour blocks. However, there have been few studies on complex-shaped objects such as Tetrapods. Smoothed Particle Hydrodynamics (SPH) is one of the most popular and has reached the maturity to be used for engineering purposes (Shadloo et al., 2016; Violeau and Rogers, 2016; Gotoh and Khayyer, 2018; Manenti et al., 2019; Tsuruta et al., 2019). SPH is an ideal method to simulate free-surface flows and violent wave-structure interactions since there is no special treatment to detect the free surface, and therefore large free-surface deformations can be efficiently treated since there is no mesh distortion. In this way, rapidly moving complex boundaries, fluid-driven bodies, and interfaces are easily treated. SPH is also a suitable numerical method capable of solving multi-body and body-fluid interactions (e.g. Asai et al., 2021). Solid-solid interactions are commonly solved using DEM, which has been coupled with SPH codes to study the sedimentation process of blocks on a seabed (Harada et al., 2011) and the behaviour of granular flows (Ikari and Gotoh, 2022). Coastal engineering problems are also solved using other SPH-based codes such as PARISPHERE code (Tsuruta et al., 2019) that is based on the Incompressible SPH (ISPH) and coupled with DEM and it includes porous model and scour model.

The SPH-based code DualSPHysics (Domínguez et al., 2022) is used in this work. DualSPHysics encourages the use of SPH for real engineering problems and can be run on either CPUs or GPUs (Graphics Processing Units with powerful parallel computing). GPUs provide high computing power and are a good option to accelerate SPH since a GPU card can also be installed on a personal computer. The source code of DualSPHysics can be freely downloaded from the website www.dual.sphysics.org. DualSPHysics has been applied widely in coastal engineering, yet mostly with fixed structures. The study of the run-up on a real armour breakwater was presented in Altomare et al. (2014), and validation with experimental data was also included in Zhang et al. (2018). Impact of tsunami bores on coastal structures was studied in St-Germain et al. (2014). Loading induced by random sea states on storm return walls was analysed in Altomare et al. (2015a), while Altomare et al. (2020) characterised the impact of extreme waves on a large-scale pier structure to evaluate the modes that determined its failure. Wave overtopping on sloping dikes was numerically measured in Altomare et al. (2021), including validation with experimental data. The capabilities of DualSPHysics to simulate freely floating objects were analysed in Canelas et al. (2015) and under the action of regular waves in Domínguez et al. (2019a). On the other hand, DualSPHysics has been coupled with the multiphysics library Project Chrono (Canelas et al., 2018; Martínez-Estévez et al., 2023), where DualSPHysics solves the fluid-object interaction in a pure SPH framework, and Chrono is employed to solve the object-object interaction in terms of surface contacts and according to material properties (Suzuki et al., 2022).

In this study, DualSPHysics is used to reproduce the hydrodynamic behaviour of the Tetrapod armour units against solitary waves, where Project Chrono is used to solve the interaction of the Tetrapod units over the mound breakwater. The case under study constitutes the application of SPH to a real problem that cannot be solved with conventional mesh-based methods. Conducting a literature review, we can find similar SPH works such as the pioneer one by Rogers et al. (2010), where the open-source code SPHysics was employed and the friction force between a moving caisson and the bed was modelled with a transition from static to dynamic friction force. Promising agreement was achieved comparing two-dimensional simulations with experimental data in terms of the displacement and the horizontal forces on the caisson. The work of Sarfaraz and Pak (2018) used the DualSPHysics code for the first time to study the stability of cubic armour blocks in low-crested breakwaters. SPH methodology was coupled with Polyhedral Discrete Element Method (DEM), which is used to solve the solid collisions. Validation included the wave force exerted onto a stationary cross-shaped block and the response of cubes under harmonic excitations (without fluid). The code was then applied to compute the forces and moments applied to each armour unit subjected to sea wave action under various conditions. However, only two-dimensional simulations were conducted in Sarfaraz and Pak (2018) and validation of the displacements of the cubes

under the wave action was not provided.

Recently, Yamamoto et al. (2022) simulated the scattering process of the armour blocks placed on the rear side of a breakwater and displaced by overflow induced by tsunami waves. Stability number for the studied armour layers (see Mitsui et al., 2014) was compared with experimental results, proving a reasonable level of accuracy for a range of hydrodynamic conditions and water levels. Moreover, the authors measured the forces exerted on the armour units in order to provide further understanding of the mechanism that leads to their displacements. The present work represents an advance in terms of numerical implementation and modelling, overcoming limitations related to the boundary conditions (DBC vs mDBC) and the fluid-object interaction solvers employed before (DEM vs Project Chrono). As mentioned before, Project Chrono is used to solve the Tetrapod-mound interaction. Besides, a more exhaustive validation is carried out in the present work, since more complete experimental data is available. The numerical results are compared with the experimental results in terms of surface elevation at different wave gauges and the displacement of the Tetrapods during the motion induced by the interaction with the different solitary waves.

An important novelty of the present study is related to the boundary conditions needed to simulate moving 3-D complex geometry, such as the Tetrapods, as briefly mentioned above. Due to the meshless nature of the SPH method, the enforcement of boundary conditions remains an open problem, since there is no unanimity in the SPH community on the best approach. The different approaches that can be found in the literature present advantages and drawbacks depending on the problem they are applied. For this reason, the SPHERIC Grand Challenge #2 (Vacondio et al., 2020) aims to encourage the development of more accurate and valid boundary conditions that can be applied to real engineering problems. However, as far as the authors know, only a few examples of 3-D fluid-driven objects with complex geometries have been simulated with SPH: i) the work of Bouscasse et al. (2013) included the simulation of a dolphin shape using ghost particles technique, although it was a 2-D geometry with no validation; ii) the Manchester Boober was successfully simulated by Omidvar et al. (2013) using repulsive forces; and iii) an impressive ditching helicopter with boundary integral approach (Macía et al., 2012) was presented by Oger et al. (2020). In this work, the geometry of the Tetrapods are treated with accuracy using a modified implementation of the Dynamic Boundary Conditions (the so-called mDBC) according to English et al. (2022), unlike the work of Sarfaraz and Pak (2018) and Yamamoto et al. (2022) that were conducted using the classical DBC.

The paper is organised as follows: Section 2 presents the main functionalities available in DualSPHysics to simulate the problem under study and describes the collision detection available in Project Chrono; Section 3 includes a brief description of the experimental campaign; Section 4 includes the numerical setup and numerical results that we compared against the experimental data (in terms of surface elevations and displacements of the Tetrapods), this section also conducts a convergence and performance analysis and applies the validated numerical tool to carry out further analysis for different coefficients of friction between Tetrapods and the mound; finally, Section 5 raises the main conclusions of this work.

2. Numerical model

This section introduces the numerical tool, where the main formulation of the Smoothed Particle Hydrodynamics (SPH) method is presented. A particular discussion is included about the implementation of the boundary conditions and the wave generation and propagation. Finally, the coupling between the open-source codes DualSPHysics and the multiphysics library Project Chrono is described. In particular, the collision detection algorithm is addressed.

2.1. SPH method

SPH is a Lagrangian meshless method where a continuum is discretised using a set of material points (or particles). In the particular case of fluid dynamics, the Navier-Stokes equations, in its discrete form, are locally integrated at the location of the particles, according to the physical properties of neighbouring particles. The contribution of those neighbouring particles depends on the distance between the particles, and the corresponding magnitude (velocity, density, etc.) is obtained using a weighted kernel function (W) with an area of influence that is defined using a characteristic length called smoothing length (h). A quintic Wendland kernel (Wendland, 1995) with compact support of radius $2h$ is applied in this study. The smoothing length (h) is defined as a function of the initial interparticle distance, dp, used to create the initial condition.

Herein, the formulation implemented in the DualSPHysics code is briefly presented. A complete view of all functionalities available in DualSPHysics v5.0 can be found in Domínguez et al. (2022).

Being a the particle where the physical quantities are being calculated and b the neighbouring particles, the system of Navier-Stokes equations (momentum and continuity equations) can be written in the discrete SPH formalism as following:

$$\frac{d}{dt}\boldsymbol{v}_a = -\sum_b m_b\left(\frac{p_b+p_a}{\rho_b\cdot\rho_a}+\Pi_{ab}\right)\nabla_a W_{ab}+\boldsymbol{g} \tag{1}$$

$$\frac{d}{dt}\rho_a = \sum_b m_b\boldsymbol{v}_{ab}\cdot\nabla_a W_{ab}+D \tag{2}$$

where W_{ab} is the kernel function, t is the time, $\boldsymbol{r}$ is the position, $\boldsymbol{v}$ is the velocity, p is the pressure, ρ is the density, m is the mass, and $\boldsymbol{g}$ is the gravitational acceleration.

The artificial viscosity (Π_{ab}) proposed in (Monaghan, 1992) is used here:

$$\Pi_{\mathrm{ab}} = \begin{cases} \left(\frac{-\alpha\overline{c_{ab}}}{\overline{\rho_{ab}}}\right)\left(\frac{h\boldsymbol{v}_{ab}\bullet\boldsymbol{r}_{ab}}{r_{ab}^2+0.01h^2}\right) & \boldsymbol{v}_{ab}\bullet\boldsymbol{r}_{ab} < 00\boldsymbol{v}_{ab}\bullet\boldsymbol{r}_{ab} > 0 \end{cases} \tag{3}$$

where c is the numerical speed of sound and h the smoothing length. The numerical results presented in this work were achieved using $\alpha = 0.04$.

On the other hand, the term D in the continuity equation introduces a diffusive term to reduce density fluctuations. The work proposed by Fourtakas et al. (2019) introduces a correction in the same formulation proposed by Molteni and Colagrossi (2009) but substituting the dynamic density with the total one.

$$D = 2\delta hc\sum_b\left(\rho_{ba}^T-\rho_{ab}^H\right)\frac{\boldsymbol{r}_{ab}\cdot\nabla_a W_{ab}}{\boldsymbol{r}_{ab}^2}\frac{m_b}{\rho_b} \tag{4}$$

being δ the coefficient that controls this diffusion term (set to 0.1 in this work) and subscripts T and H represent the total and hydrostatic component of the density of a weakly compressible and barotropic fluid by locally constructing the hydrostatic pressure as:

$$\rho_{ab}^H = \rho_0 g z_{ab} \tag{5}$$

where z_{ab} is the vertical distance between particles a and b.

As pointed out by Fourtakas et al. (2019) this formulation improves the behaviour of pressure near the wall boundaries, when compared with the formulation proposed by Molteni and Colagrossi (2009) and, at the same time, it avoids the high computational cost associated to the calculation of the normalized density gradient in delta-SPH proposed in Antuono et al. (2012). Thus, despite the formulation of Antuono et al. (2012) is more general, the formulation by Fourtakas et al. (2019) can be satisfactorily used for gravity-dominated flows.

The fluid is treated as weakly compressible in DualSPHysics, so that

an equation of state is used to calculate fluid pressure as a function of density rather than solving a Poisson-like equation. In fact, the compressibility is adjusted to reduce the speed of sound so that the time step (based on the sound speed) are reasonable. Therefore, the system of equations presented before is closed with the Tait's equation of state:

$$p = \frac{c^2 \rho_0}{\gamma}\left[\left(\frac{\rho}{\rho_0}\right)^{\gamma} - 1\right] \tag{6}$$

where $\gamma = 7$ is the polytropic constant, with $\rho_0 = 1000$ kg/m^3 being the reference density of the fluid.

The meaningful magnitudes (position, velocity, density and pressure) are integrated in time using a symplectic algorithm (Leimkuhler and Matthews, 2015). The symplectic position Verlet time integrator scheme is second order accurate in time. It is ideal for Lagrangian schemes as it is time reversible and symmetric in the absence of diffusive terms that preserve geometric futures. The position Verlet scheme in the absence of dissipation forces reads:

$$\boldsymbol{r}_a^{n+\frac{1}{2}} = \boldsymbol{r}_a^n + \frac{\Delta t}{2}\boldsymbol{v}_a^n \tag{7.1}$$

$$\boldsymbol{v}_a^{n+1} = \boldsymbol{v}_a^n + \Delta t \frac{d\boldsymbol{v}_a^{n+\frac{1}{2}}}{dt} \tag{7.2}$$

$$\boldsymbol{r}_a^{n+1} = \boldsymbol{r}_a^{n+\frac{1}{2}} + \frac{\Delta t}{2}\boldsymbol{v}_a^{n+1} \tag{7.3}$$

However, in the presence of viscous forces and density evolution in DualSPHysics, the velocity is required at the $(n+1/2)$ step thus, a velocity Verlet half step is used to compute the required velocity for the acceleration and density evolution for $d\boldsymbol{v}/dt(\boldsymbol{r}_{n+1/2})$ and $d\rho/dt$ $(\boldsymbol{r}_{n+1/2})$, respectively. The scheme implemented in DualSPHysics follows:

$$\boldsymbol{r}_a^{n+\frac{1}{2}} = \boldsymbol{r}_a^n + \frac{\Delta t}{2}\boldsymbol{v}_a^n \tag{8.1}$$

$$\boldsymbol{v}_a^{n+\frac{1}{2}} = \boldsymbol{v}_a^n + \frac{\Delta t}{2}\frac{d\boldsymbol{v}_a^n}{dt} \tag{8.2}$$

$$\boldsymbol{v}_a^{n+1} = \boldsymbol{v}_a^n + \Delta t \frac{d\boldsymbol{v}_a^{n+\frac{1}{2}}}{dt} \tag{8.3}$$

$$\boldsymbol{r}_a^{n+1} = \boldsymbol{r}_a^n + \Delta t \frac{\boldsymbol{v}_a^{n+1} + \boldsymbol{v}_a^n}{2} \tag{8.4}$$

where $\boldsymbol{r}^{n+1/2}$ is substituted to $\boldsymbol{r}^{n+1}$ in eq. (7) to eliminate dependence from $\boldsymbol{v}^{n+1/2}$. Finally, the density evolution follows the half time steps of the symplectic position Verlet scheme as follows (Parshikov et al., 2000):

$$\rho_a^{n+\frac{1}{2}} = \rho_a^n + \frac{\Delta t}{2}\frac{d\rho_a^n}{dt} \tag{9.1}$$

$$\rho_a^{n+1} = \rho_a^n \frac{2 - \varepsilon_a^{n+\frac{1}{2}}}{2 + \varepsilon_a^{n+\frac{1}{2}}} \tag{9.2}$$

where $\varepsilon_a^{n+\frac{1}{2}} = -\left(\frac{d\rho_a^{n+\frac{1}{2}}}{dt} / \rho_a^{n+\frac{1}{2}}\right)\Delta t$.

A variable time step is used in DualSPHysics based on the CFL (Courant-Friedrich-Lewy) condition, the force terms and the viscous diffusion term following Monaghan et al. (1999).

2.2. Boundary conditions

Dynamic Boundary Conditions (DBC) (Crespo et al., 2007) have been initially implemented in DualSPHysics. Solid objects such as the walls and bottom of flow facilities, floating objects, wavemakers, hydraulic and maritime structures, etc., are discretised by a set of boundary particles that satisfy the same equations as fluid particles, however they do not move according to the forces exerted on them. When a fluid particle approaches a boundary particle, and the distance becomes smaller than the interaction distance ($2h$), the density of the affected boundary particles increases, resulting in a pressure increase. In turn, this results in a repulsive force being exerted on the fluid particle due to the pressure term in the momentum equation. DBC have been successfully applied in some coastal engineering problems due to their capability of discretising complex 3-D geometries into a set of boundary particles, as presented in the study of wave-runup of armour block breakwaters (Altomare et al., 2014; Zhang et al., 2018). However, DBCs present some drawbacks, such as an over dissipation that leads to un-physical large boundary layers. A modification of DBC (the so-called mDBC) has been presented by English et al. (2022). Within this implementation, the boundary particles are arranged in the same way as in the original DBCs, but with the boundary interface located at a given distance away from the innermost layer of boundary particles (defined as $dp/2$ for simple geometries). Boundary interface is represented as a solid black line in Fig. 1. For each boundary particle, a ghost node (red cross in Fig. 1) is created in the fluid domain in a similar way as Marrone et al. (2011). This ghost node is projected according to the normal vector of the boundary pointing to the fluid part of the domain (arrows in Fig. 1). For a flat boundary, the ghost node is mirrored across the boundary interface along the direction of the normal pointing into the fluid. For boundary particles located in a corner, the normal is defined as the direction between the boundary particle and the corner, so that the ghost node is mirrored through the point of this corner into the fluid domain. Fluid properties are then computed at the ghost node through a corrected SPH approximation and finally mirrored back to the boundary particles. Density field at the ghost node is computed according to Liu and Liu (2006). This new approach is here applied since it provides a more accurate and smoother pressure field, resulting in a reduction of the unphysically large boundary layer, as already shown in English et al. (2022).

Rigid bodies, such as the units of the armoured breakwater, are discretised as a set of particles where the mDBC approach is applied, and their motion can be obtained by solving the basic equations of the rigid body dynamics, where the net force of each floating particle is computed first as the summation of the contributions of all surrounding fluid particles (Canelas et al., 2015).

2.3. Wave generation

Different techniques to generate sea waves have been implemented in DualSPHysics, such as i) the use of boundary particles, mimicking the displacement of the piston- and flap-type wavemakers that move following 1st and 2nd order wave generation solution for regular and random waves (Altomare et al., 2017) and solitary waves (Domínguez

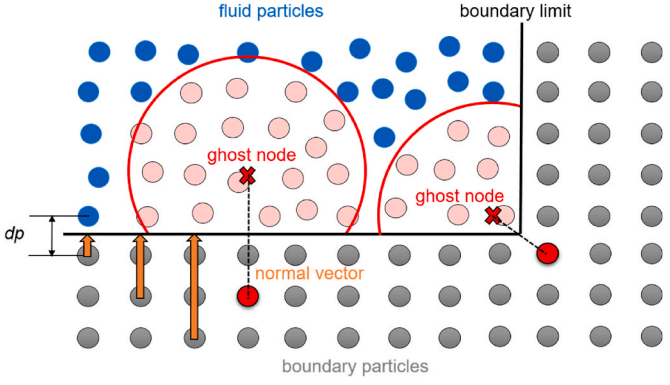

Fig. 1. Projection of ghost nodes by mirroring the boundary particles according to the normal vector of the boundary pointing to the fluid domain (for a flat surface and corner).

et al., 2019b), ii) relaxation zones (Altomare et al., 2018) employed either as stand-alone generation method or as coupling method with other phase-resolving models, iii) inlet/outlet open boundaries (Verbrugghe et al., 2019) developed initially for two-way coupling with wave propagation models but also suitable for stand-alone wave generation, and iv) multi-layered piston wavemaker (Altomare et al., 2015b) coupled with external method (hereafter called ML-piston). This last method is the one employed in the present simulations. The ML-piston consists of a set of boundary particles that are bound together however they do not move as a whole rigid body, but rather have horizontal movements, which are reconstructed on the basis of the velocity time series that have been previously resolved in SWASH model (Zijlema et al., 2011) or any other model employed for wave propagation. In this work, OpenFOAM is employed for the purpose. The first model provides information of the velocity field along the water depth at a specified location along the wave propagation (i.e. coupling location), allowing accurately reconstructing the velocity profile in DualSPHysics. For models like SWASH this means to work in a multi-layered mode, while models like OpenFOAM provides velocity field for each mesh or nodal point that discretises the depth. The velocity time series reconstructed at each point along the water depth are then interpolated to assign velocity to each boundary particle of the ML-piston. This coupling technique is a 1-way offline coupling with no reflection compensation, for which it is suitable only for low-reflective cases or very short time series used, such as the modelling of the main pulse of a single solitary wave.

2.4. Project Chrono library

The Project Chrono library (Tasora et al., 2016) is coupled with DualSPHysics to solve the fluid-structure interaction problem with mechanical constrains applied on rigid bodies. A first description and validation of the coupling between DualSPHysics and Chrono can be found in Canelas et al. (2018), where a simply supported platform was exposed to a dam break leading to the collapse and partial transport of the structure. Moreover, the same authors presented a new structured version of the DualSPHysics code coupled to the multiphysics library using a co-simulating environment in Martínez-Estévez et al. (2023), improving the applicability to industrial problems. A rigorous validation of the collision detection algorithm has been already conducted in Martínez-Estévez et al. (2023), following the experimental setup proposed in Hagemeier et al. (2021). Good agreement was found between the numerical vertical component of a fully submerged sphere falling down and impacting the bottom surface of the tank made of steel.

The smooth dynamics model, available in Project Chrono, deals with discontinuous frictional contacts and kinematic restrictions. The first ones are of interest in this work since the interaction between the different Tetrapods of the breakwater and those Tetrapods interacting with the mound are solved by that collision detection algorithm. In particular, the smooth contact code implemented (single-core) in Chrono 4.0.0 module is used in this work. The collision detection is activated when the distance between two approaching objects is less than a minimum distance defined by the user. Therefore, Project Chrono uses the outer envelope surface of those objects to detect collisions in terms of surfaces (not in terms of particles). The normal force ($\boldsymbol{F}_n$) is solved using the following expression:

$$\boldsymbol{F}_n = k_n \delta_n^{3/2} \widehat{\boldsymbol{n}} - c_n \delta_n^{3/2} \boldsymbol{v}_n \tag{10}$$

where k_n is the normal stiffness, c_n is the normal damping, $\boldsymbol{v}_n$ is the normal component of the relative velocity at the point of contact, δ_n is the normal overlap, and $\boldsymbol{n}$ is the unit vector pointing from one particle centre to the other (or from one surface object to the other). Note that values of normal stiffness and damping depend on the user definition of the material properties like Young's modulus, Poisson's ratio and coefficient of restitution. On the other hand, the tangential force ($\boldsymbol{F}_t$) follows the Coulomb friction condition that defines a maximum allowable force $|\boldsymbol{F}_{t,max}| = \mu_s |\boldsymbol{F}_n|$, but it can be written in a general way as:

$$\boldsymbol{F}_t = min\left[\mu_s |\boldsymbol{F}_n| \frac{\boldsymbol{\delta}_t}{|\boldsymbol{\delta}_t|}, -k_t \delta_n^{1/2} \boldsymbol{\delta}_t - g_t \delta_n^{1/4} \boldsymbol{v}_t\right] \tag{11}$$

with μ_s as the coefficient of static friction that defines when passing from tangential sticking to tangential slipping, k_t is the tangential stiffness, $\boldsymbol{v}_t$ is the tangential component of the relative velocity at the point of contact, and δ_t is the tangential displacement vector. The normal and tangential forces computed on each body as result of the collision are included in the basic equations of the rigid body dynamics in order to compute the final motion of the solids. A complete description of the formulation can be found in Sunday et al. (2020).

Based on the above-described approach, the friction coefficient between different Tetrapods and the friction coefficient between them and the mound of the breakwater needs to be defined for the materials that collide. In this research, the values measured during the experimental campaign are used. However, it should be mentioned that the contact models implemented in the version of Project Chrono used here, do not consider the kinetic friction coefficient and the solver only accounts for the initial static friction coefficient (μ_s), which is also used when the rigid body is already moving.

3. Experimental campaign

A series of physical tests to analyse the movement of Tetrapods units against solitary waves were carried out in the facilities of Fudo Tetra Corporation in Japan. In this research, some of those tests are chosen to validate the numerical tool where the displacement of the units during the simulation is compared with physical experiments, as shown in the following sections.

A wave flume of 55 m in length, 1.2 m in width, and 1.5 m in height was used for the experiments. The facility is equipped with a piston-type wave generator. The layout of the flume is shown in Fig. 2. The position of the experimental wavemaker in the pulled state was defined as $x = 0$ m. A fixed seabed of mortar with a slope of 1/30 was built from $x = 19.0$ m (19 m from the wave paddle). A foundation mound and Tetrapods were installed at $x = 39.0$ m on the slope. The water depth was 0.80 m at the offshore uniform depth and 0.083 m at the centre of the structure.

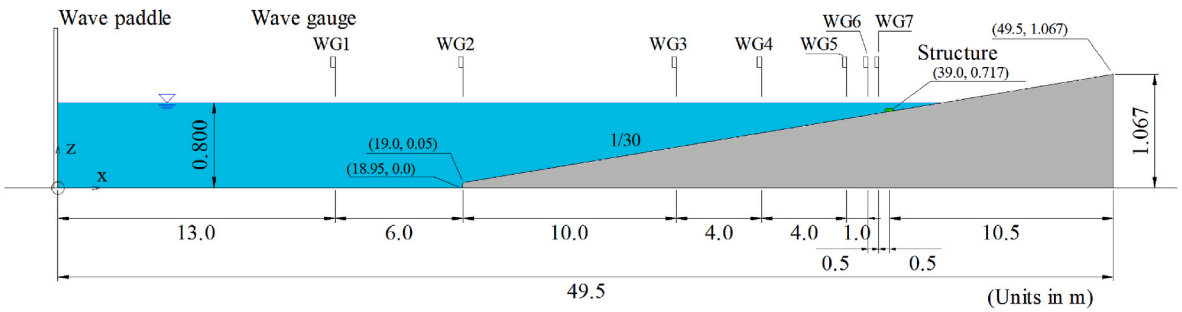

Fig. 2. Layout of the wave flume during the experiment.

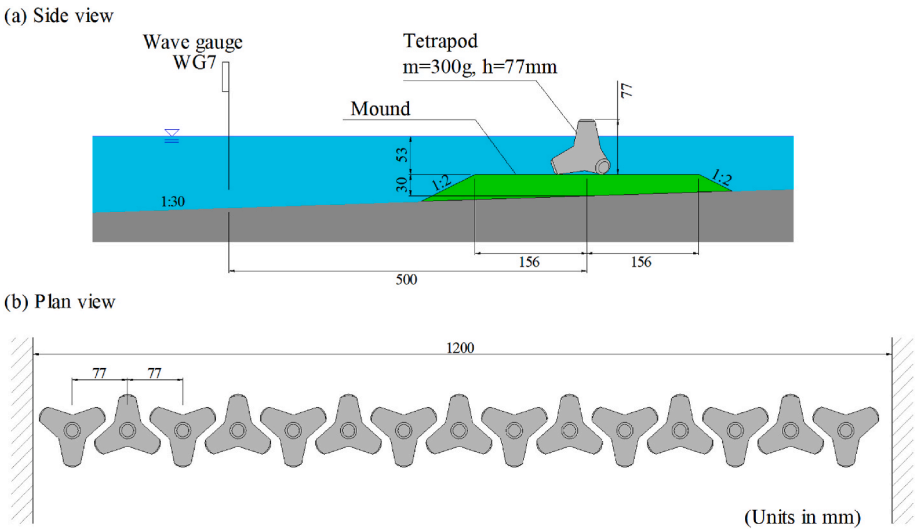

Fig. 3. Side view and plan view of the structure.

Wave gauges were installed at seven locations (WG1 to WG7) to measure the water surface elevation.

The Tetrapods are regularly placed in a single row on the mound, as shown in Fig. 3. The Tetrapod model (scale was assumed to be 1:50) was made of mortar, 7.7 cm in height, 126 cm^3 in volume and 0.3 kg in mass, resulting in a density of 2.38 g/cm^3. The friction coefficient between Tetrapods is 0.65. The mound was impermeable, with a polyvinyl chloride (PVC) panel attached to the mound surface. The friction coefficient between PVC and the blocks was measured prior to the experimental campaign as following described.

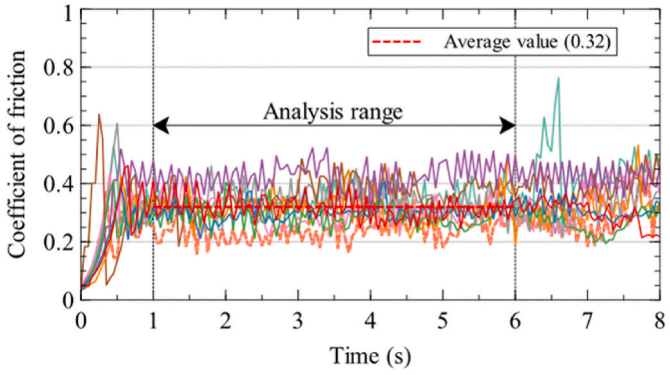

Fig. 4. Measurements of the coefficient of friction in the laboratory.

A Tetrapod model was placed on a shallow container with a PVC panel attached, and the load was measured by pulling it horizontally with a nylon string. The force gauge was pulled at a speed of about 1.2 cm/s. The shallow container was filled with a thin layer of water to maintain the wet condition. The measurements were repeated 10 times. Fig. 4 shows the time series of the friction coefficient calculated by dividing the pulling force by the self-weight of the block. The average value for 5 s, excluding 1 s at the start of the movement, was calculated, and 0.32 was obtained as the average of the 10 measurement results. The friction coefficient obtained in this way is used in the numerical simulations.

The experiments on block movement due to solitary wave action was carried out as follows. The wave heights of the solitary waves were varied to 2.6 cm, 4.5 cm, and 6.4 cm at the offshore uniform depth (WG1 in Fig. 2). Hereinafter, the three different waves are named according to the wave height at WG1. The number of moved blocks and the displacement of each block were measured. In this study, the blocks that moved more than one block height (7.7 cm) defined a damage condition, and the damage rate was calculated. The displacement distance was obtained by analysing the images taken by a video camera from above. The blocks were placed again at the initial position after each wave action. The experiment was repeated three times at each wave height rank. Fig. 5 shows the movement of the blocks after the solitary wave action. It was observed that the blocks slid toward the shore and fell off the mound in the case of large wave height. The results of the first of

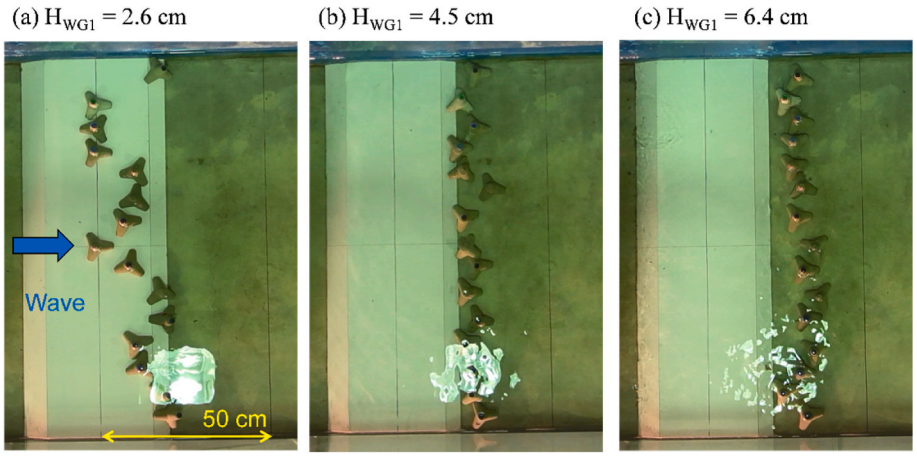

Fig. 5. Displacement of the blocks after the solitary wave action.

three repetitions of the experiment are shown.

The experimental time series of the water surface elevation (η) is shown in Fig. 6. It can be seen how the wave height increases as it is propagated along the slope (the wave is shoaling), but in all cases, the wave acted on the Tetrapods before breaking.

4. Results

The physical model tests where one row of Tetrapods were placed on the mound of PVC are reproduced with the numerical model for the different solitary wave conditions. The numerical results presented here were all obtained using the latest version of the coupling between the open-source codes DualSPHysics (v5.0 is available for free download at https://dual.sphysics.org/downloads/) and the multiphysics library Project Chrono (v4.0.0 is also available at https://projectchrono.org/download/). The numerical setup is explained first, where special attention is paid to the boundary conditions used to discretise the complex geometry of the Tetrapods and to the wave generation of the solitary waves. Then, a detailed validation is presented with comparisons of the: i) analytical and numerical hydrostatic force exerted by the fluid onto the semi-submerged blocks, ii) numerical response between Tetrapod and PVC-slope using the friction coefficient that was measured experimentally, iii) experimental and numerical surface elevation at different wave gauges, iv) experimental and numerical displacement of the Tetrapods during the motion induced by the interaction with the different solitary waves. This section also includes a convergence and performance analysis that helps to decide the best numerical resolution in terms of accuracy and computational runtime. Finally the validated model is used to study the effect of the roughness of the mound.

4.1. Numerical setup

The numerical tank needs to be defined to mimic the physical facilities. In this way, the dimensions of the experiment (Figs. 2 and 3) are used to create the numerical system. Note that the width of the wave flume in the physical experiment and in the simulations is the same (1.2 m), being the total number of Tetrapods (15) in the experiment modelled with DualSPHysics. However, the flume length of the numerical SPH domain is reduced compared to the experimental one. In fact, a mesh-based CFD tool is first executed in order to propagate waves and use the information at 6 m from the mound to generate solitary waves in the reduced SPH domain (this will be explained better in the following sub-section).

In order to discretise the numerical domain described before into particles, an initial interparticle distance, dp, needs to be first defined. Following the recommendations in Altomare et al. (2017) and Rota-Roselli et al. (2018), a minimum of 5 particles need to be used to define the wave height (H) for accurate wave propagation ($H/dp > 5$). According to the minimum wave height measured at WG1 (Fig. 6), $dp = 0.005$ m was initially considered, which means that H/dp is 5, 9 and 13 for the three different solitary wave heights at WG1. Moreover, using this resolution, 15 particles were created in the characteristic size of a

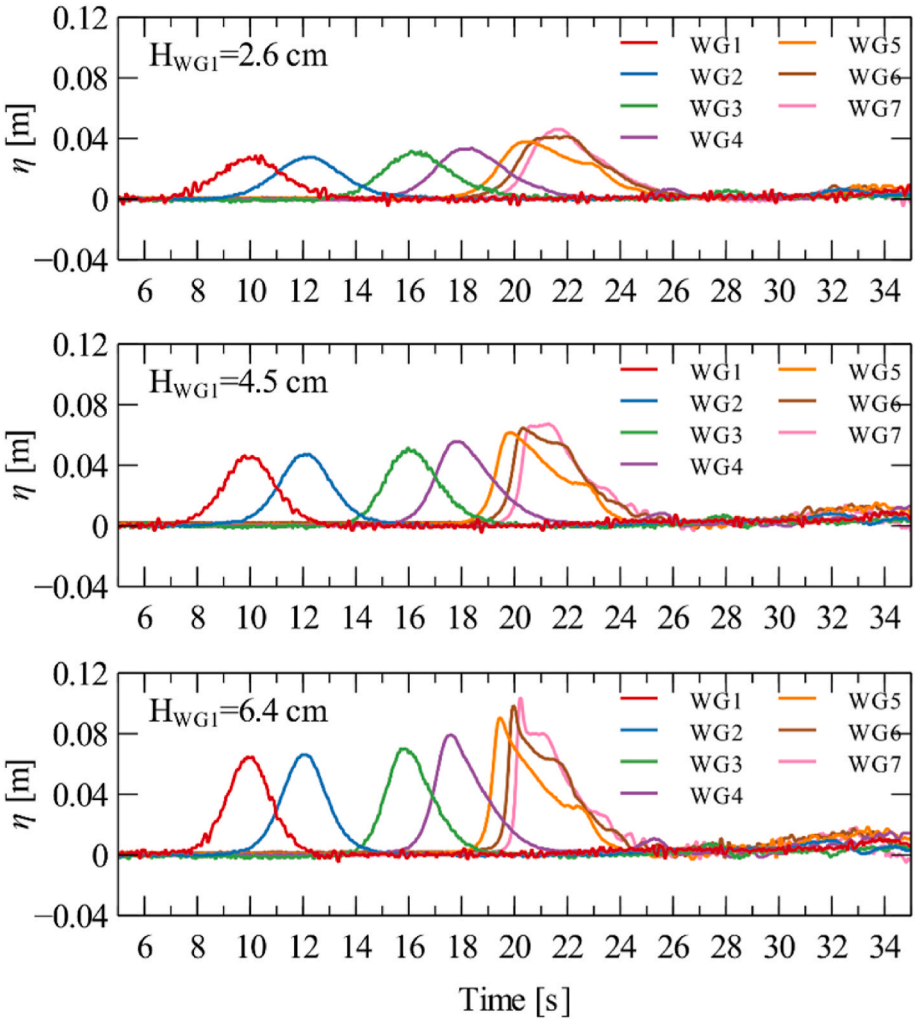

Fig. 6. Time series of the experimental water level.

Tetrapod (7.7 cm). Note that the DualSPHysics software suite includes pre-processing tools that allow to introduce complex geometries by means of a wide range of input files including CAD, STL, PLY files, etc., making the setup of simulations straightforward. In this case, the actual geometry of the Tetrapods can be used using STL files.

The distance of interaction (kernel radius) is here defined as $2h = 0.021$ m (being $h = 1.2 \cdot \text{sqrt}(3) \cdot dp$, in 3D). A total number of 17,541,570 particles are created with 15,385 particles discretising the 15 Tetrapods (Table 1). The simulation of 20 s of physical time took around 30 h (for the three solitary wave conditions) using NVIDIA GeForce RTX 3080Ti GPU with Intel i7-8700K CPU and 64 GB RAM. Around 4 h of that total execution time was consumed by Project Chrono solving the interactions between Tetrapods and mound with Tetrapods. Whereas the DualSPHysics is executed on the GPU card, the collision detection of the Project Chrono library is executed on single-core CPU (Martínez-Estévez et al., 2023). A convergence study is also conducted in this work, where different numerical resolutions and runtimes will be analysed in Section 4.6.

As mentioned in Section 2.2, the new mDBC are used here to simulate the boundary particles (wavemaker, mound, tank and blocks). In order to apply mDBC, normal vectors created for each particle with direction towards the boundary interface (STL faces) are needed, their module being the distance between the position of the boundary particle and boundary interface (see Fig. 1). Note that normal direction and module are key to obtaining the ghost node projected into the fluid across that boundary interface. Fig. 7 includes the STL file of a Tetrapod (a), how this is discretised into SPH boundary particles (b) and the result of computing normal vectors (c) for each particle. The module of each normal vector varies depending on the distance between the particle and the boundary interface (STL) as shown in Fig. 1. This is the first time that mDBC is applied to such a complex geometry as the Tetrapod one. The use of mDBC, as it was proven in English et al. (2022), avoids the large boundary layer created when using DBC so that fluid-structure interaction is accurately solved. On the other hand, the geometry of the Tetrapods needs to be properly discretised into particles (here we use $dp = 0.005$ m) in order to numerically reproduce the actual volume of the unit, so that, the actual buoyancy force.

Table 1
Computational times for the simulations of 17,541,570 particles (15,385 floating particles).

Configuration	Runtime SPH + Chrono	Runtime Chrono
$H_{WG1} = 2.6$ cm	29.90 h	3.95 h
$H_{WG1} = 4.5$ cm	30.42 h	4.34 h
$H_{WG1} = 6.4$ cm	30.44 h	4.09 h

4.2. Validating wave propagation with ML piston

A vertical 2-D analysis was performed first for the entire wave flume, and then the result was connected to a 3-D analysis for a small domain including the structure using one-way coupling (see Fig. 2). The vertical 2-D analysis was performed using OpenFOAM-v1712. A solver named interDyMFoam was used, which is a Volume Of Fluid (VOF) solver for gas-liquid two-phase flow with moving grid functionality. A vertical wall boundary was created in the analysis domain to simulate a wave maker, and a solitary wave was created by moving the wall boundary toward the shore using the moving grid function, as in the experiment. The moving speed of the wavemaker was calculated by the method by Goring and Raichlen (1980) using the measured wave height at the uniform water depth (WG1) obtained from physical experiments. The grid size was set to 2 cm in the horizontal direction and 1 cm in the vertical direction from the offshore end to $x = 19.0$ m, and 1 cm in both the horizontal and vertical directions on the shore side. The grid was further subdivided by half near the still water surface on the shore side from the $x = 27.0$ m. The time increments were set to be variable so that the maximum Courant number would be less than 0.35. To connect to the 3-D analysis, the water particle trajectories at the connection point were output in order to get the time series of the position and the velocity at those positions. The 3-D analysis by DualSPHysics was conducted for the region closer to the mound. Hence, a wave maker was installed at 6 m from the mound and moved using the ML-piston. The time series of the vertical position and horizontal velocity obtained with the 2-D mesh-based code were given to move the wavemaker in the SPH simulations. Note that although OpenFOAM cannot be used for the main purpose of this work, which is to study the movement of the Tetrapods under the action of different solitary waves, however, it is used to propagate waves in a large numerical flume. The ML-piston used in the SPH domain can be moved with the information provided by any other efficient model of wave propagation such as SWASH, OceanWave3D, etc.

A comparison of the experimental and numerical time series of the water surface elevation (η) at the locations of WG5, WG6 and WG7 is shown in Fig. 8. Note that the location of WG7 is placed in front of the structure (Fig. 2). The results show good agreement at all wave height ranks. In particular, the case of $H_{WG1} = 6.4$ cm has a sharp waveform just before the wave breaking, and the water level peak for a short time also agrees well. These results confirm the validity of the analysis method for the propagation of the solitary wave, which connects the vertical 2-D analysis by the VOF method to the 3-D analysis with a reduced domain by the SPH method using ML piston.

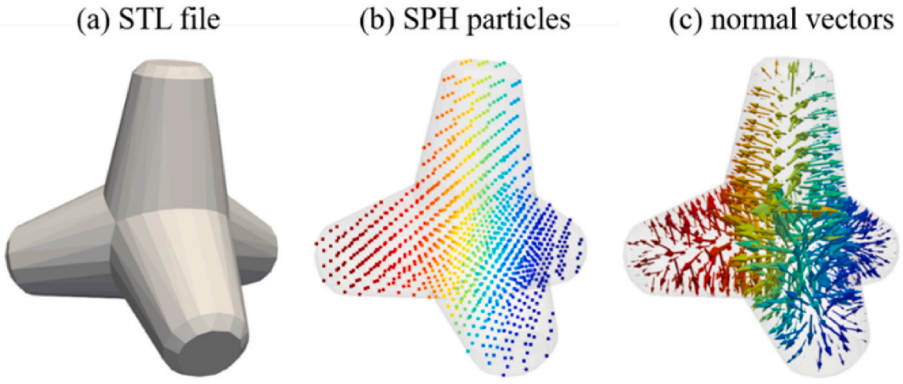

Fig. 7. Complex geometry of the Tetrapod: STL file (a), discretization into particles (b) and computation of normals (c) required to apply projections for mDBC approach.

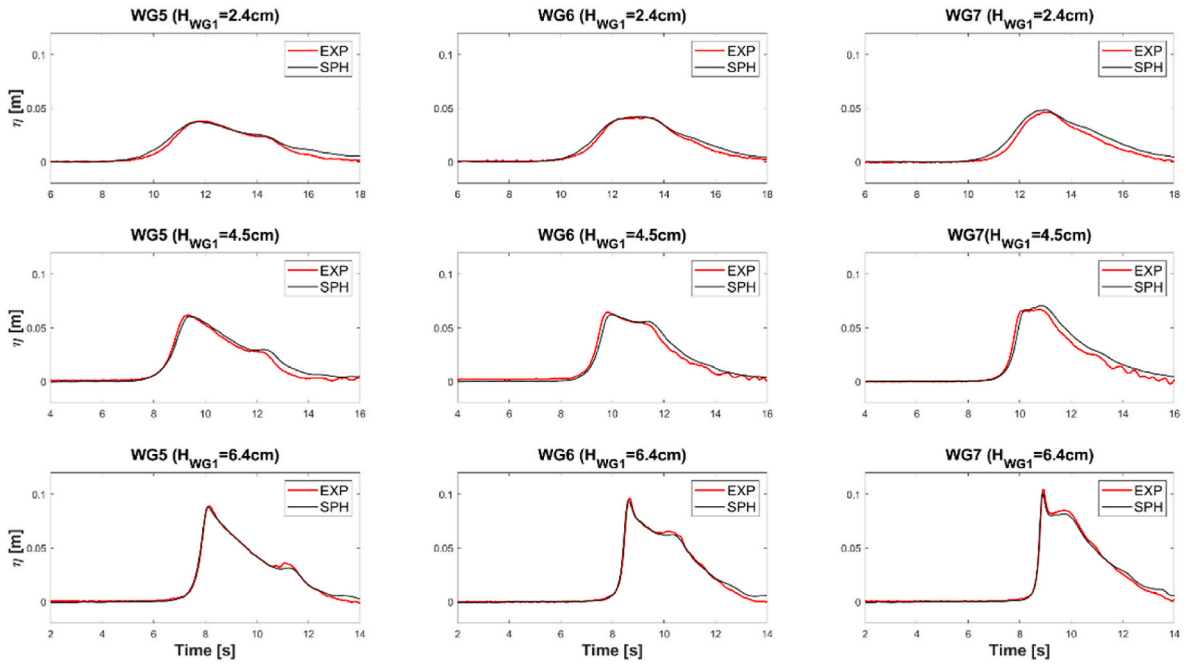

Fig. 8. Time series of experimental and numerical water level at three different wave gauges (WG5, WG6, WG7).

4.3. Validating friction with Project Chrono

Note that the actual values of the friction coefficient between Tetrapods (mortar) of 0.65 and between Tetrapods (mortar) and mound (PVC) of 0.32 are used in the simulations. Therefore, the first validation of Project Chrono itself was carried out in order to check the numerical results of the collision detection algorithm. In these tests, only solid objects are included: one Tetrapod is resting on a horizontal plane that starts rotating. As input information for these simulations, the exact geometry of the unit is given, the mass of each Tetrapod (0.3 kg) and the values of friction to be tested (0.32 and 0.65). The instant, so that the angle, when the Tetrapod starts to slide along the plane is used to determine the numerical friction coefficient as the tangent of the angle. Results of this new validation are shown in Table 2, where it can be noted that the error of the numerical results is less than 2%.

4.4. Validating displacement and damage of Tetrapods with the coupled model

The results of the full simulations are presented hereafter. The coupled code between DualSPHysics and Project Chrono is used to reproduce the physical tests with one row of Tetrapods over a mound made of PVC. Fig. 9 presents a first visual comparison with images of the first repetition of each experiment on the left and snapshots of the simulation on the right side (lateral views). The first frames (a) correspond to the initial situation before the arrival of the wave, while the rest of the images show the final instant after the solitary wave has already interacted with the Tetrapods. In this way, the displacement of the blocks can be observed for each wave condition: H_{WG1} = 2.6 cm (b), H_{WG1} = 4.5 cm (c) and H_{WG1} = 6.4 cm (d).

Table 2
Analysis of the coefficient of friction simulated in Project Chrono.

Parameter	PVC-Mortar	Mortar-Mortar
Experimental friction coefficient	0.320	0.650
Numerical angle of the slope	0.315 rad	0.585 rad
Numerical friction coefficient *tan(angle)*	0.326	0.662
ERROR	+1.8%	+1.9%

Fig. 10 shows the same results as in Fig. 9 but this time with a top view, where the total displacement of the numerical and experimental Tetrapods can be more noticeable. In order to validate the numerical tool with these physical tests, the displacements of the blocks are obtained numerically and compared with the experimental data. It can be noted that the behaviour of the different blocks is quite symmetrical in DualSPHysics, while in the experiments it is not. One of the reasons may be due to the fact that the mound in the numerical model is homogenous along the width direction. On the contrary, there might be small differences and variations in the experimental model, so that, locally, the roughness of the mound is not the same along the whole flume width. Even, blocks may be slightly different in the experiment.

It is worth mentioning again that three different repetitions were carried out during the experimental campaign and it was noted that an important difference among them is the initial disposition of the Tetrapods. Fig. 11 plots the two different initial configurations for one row that can be simulated, where the orientation of the units is reversed. Therefore, it is important to compare the final displacement of the three physical tests (EXP1, EXP2 and EXP3) with two different configurations of the simulations (SPH1 and SPH2). The initial configuration during the three experimental repetitions was random and not defined beforehand, consequently EXP1, EXP2 and EXP3 are just three different tests of the same setup, while SPH1 and SPH2 are the same simulations but with two initial orientations.

Fig. 12 compares the individual displacement of the 15 Tetrapods during the three repetitions of the experiments with the two numerical configurations (Fig. 11) for each wave condition. Analysing first the two highest waves (H_{WG1} = 4.5 cm and H_{WG1} = 6.4 cm), the experimental and numerical displacements are in agreement. In fact, there is not much variation in the displacement of the 15 Tetrapods of the same test or simulation. However, the case of H_{WG1} = 2.6 cm is different, and looking first at the experimental displacements, it is clear that a high variation

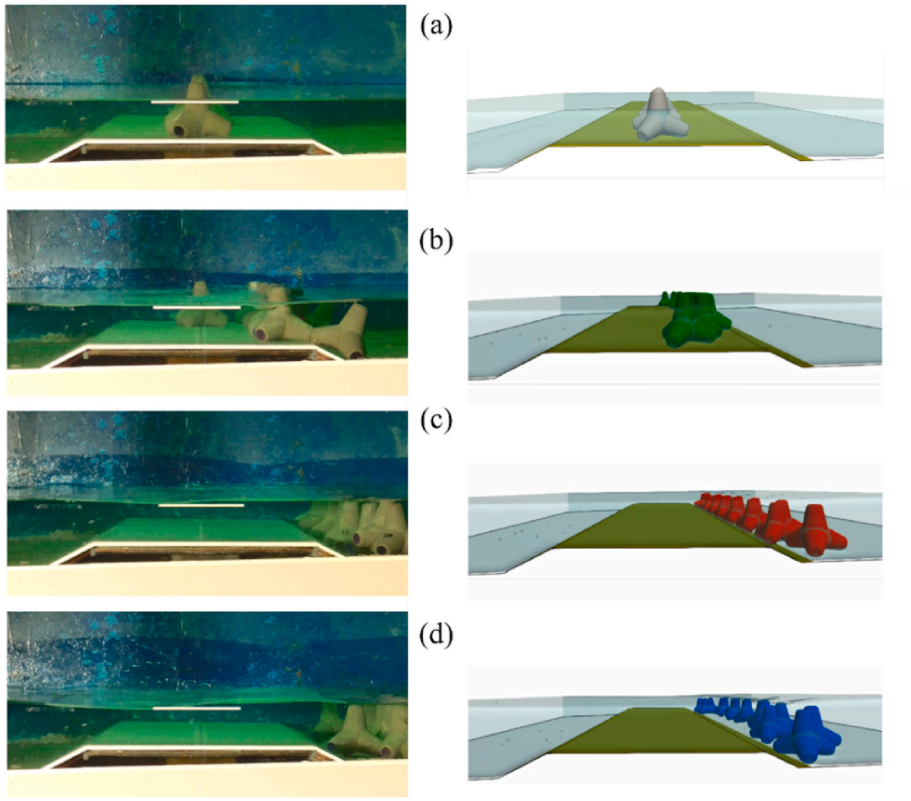

Fig. 9. Lateral view of the initial (a) and final situation of the Tetrapods after the interaction with the three different solitary waves (b,c,d) during the experiments (left) and with the numerical simulations (right).

was measured along the units, while the numerical displacements show less deviation. Appendix A includes the individual displacement values in the form of tables for the three solitary wave conditions. Average and standard deviation values are also computed and, for the lowest wave condition, a very high deviation is obtained for the experiments.

After visual comparison and in order to measure the discrepancies, the average values of the displacements have been quantified and are presented in Table 3. First, the average of the displacements of the Tetrapods during experiments is computed for each repetition (EXP1, EXP2, EXP3) and the average of the three repetitions was computed again in order to obtain one experimental value of displacement for each solitary wave (EXP), that are compared with the numerical average of SPH1 and SPH2 (Fig. 11). Table 3 includes all these data and the error between experimental and numerical solutions. Errors smaller than 1% are achieved for the three solitary wave conditions, but we should keep in mind the difficulties to reach high reproducibility in the experiments, where even for the largest wave height EXP3 showed a large deviation from EXP1 and EXP2. Besides, for $H_{WG1} = 2.6$ cm, where the lowest hydrodynamic forces are at skate, high standard deviation was registered for the individual displacements (Appendix A).

From a practical point of view, it is interesting to quantify the rate of damage, besides the unit displacement. As mentioned in Section 3, damage rate is defined as the number of blocks that moved more than the characteristic size (7.7 cm) over the total number of blocks. Results can be found in Table 4, which includes the damage rate of each individual repetition of the experiments, the average of the three repetitions and the numerical value. All blocks move more than 7.7 cm for the cases with $H_{WG1} = 4.5$ cm and $H_{WG1} = 6.4$ cm, so that damage is 100% both during the experiment and in the simulations. Note that in the case of $H_{WG1} = 2.6$ cm, the 15 Tetrapods in the simulations were moved, but two are moved less than 7.7 cm, so they are not included in the damage computation (86.67%).

Experimental and numerical displacements and damage are also represented in Fig. 13 using bar charts. Displacements and damage of the two simulations and three experiments are included in the figure. Overall, the numerical values agree with the experimental data. It can be concluded that the DualSPHysics model coupled with the Project Chrono library can reproduce the hydrodynamic response of Tetrapods with an acceptable level of accuracy, at least for the configuration of one row of blocks made of mortar over a PVC mound and against the three solitary wave conditions simulated here.

4.5. *Hydrodynamic field study with the numerical model*

There is no experimental information regarding the flow field, however the numerical model allows us to compute the pressure and velocity field and the forces exerted onto the Tetrapods by the solitary waves. In this way, the time series of the wave force experienced by the units is shown in Fig. 14. For the sake of clarity, the average of the fifteen-time series of the forces exerted on the fifteen Tetrapods are included, including the standard deviation, which is represented with the shaded area. Total force is represented here without the initial hydrostatic force: the one due to the initial partially submerged situation of the units. Considering the different wave conditions, it can be observed how the maximum forces increase with wave height as it is expected. A peak in the force signal appears and is more evident for larger waves.

The force peak corresponds to the instant when the solitary wave is reaching the units and passing over their crest. The presence of the units induces a prompt change of the wave steepness and wave momentum. For the largest wave this will lead to wave breaking after the passage over the tetrapods. The force time-series corresponds to the case of slightly-breaking waves presented by KortenhausOumeraci (1998), albeit defined for vertical structures, with the ratio between the peak and the following quasi-static part of the signal is smaller than 2.5. The wave crest provides the unit's displacements with consequent reduction of the hydrodynamic force acting on them. After the main wave pulse, the force does not return to zero: the bump on the trail is actually caused by the Tetrapods falling down of the mound, so finding themselves in larger water depth than the initial one (excess of hydrostatic components with respect to the initial position).

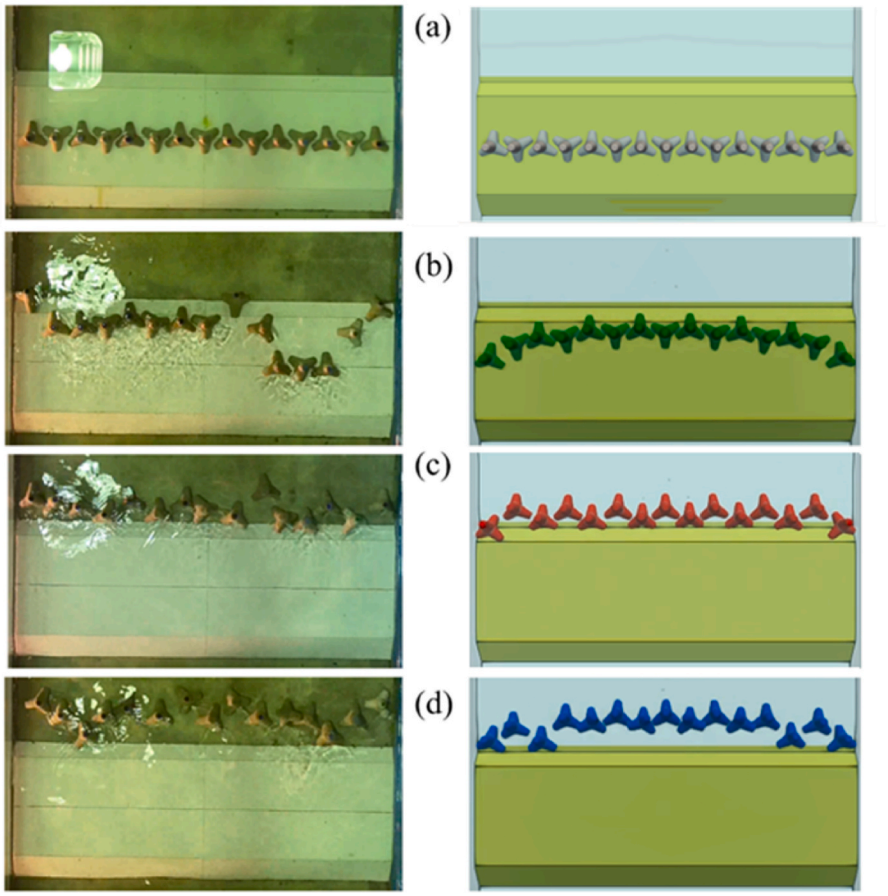

Fig. 10. Top view of the initial (a) and final situation of the Tetrapods after the interaction with the three different solitary waves (b,c,d) during the experiments (left) and with the numerical simulations (right).

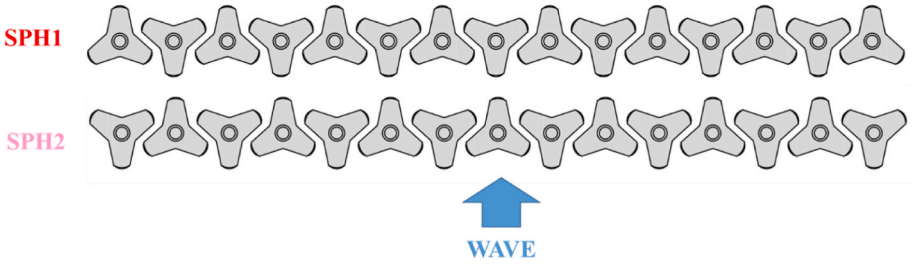

Fig. 11. Two different configurations can be simulated according to the initial orientation of the Tetrapods.

Moreover, the pressure and velocity field during the interaction of $H_{WG1} = 4.5$ cm with the central Tetrapod (unit 8) is plotted in Fig. 15. Note that a cross-sectional view of 16 mm is represented here where around 3 particles size ($dp = 0.005$ m) are visualised in the width direction. In the left panels, colour of the particles corresponds to the pressure value of each individual fluid particle, considering that values from 0 to 1000 Pa follows a water column of 0.1 m. Several instants are depicted in the figure, that correspond to the arrival of the wave in the

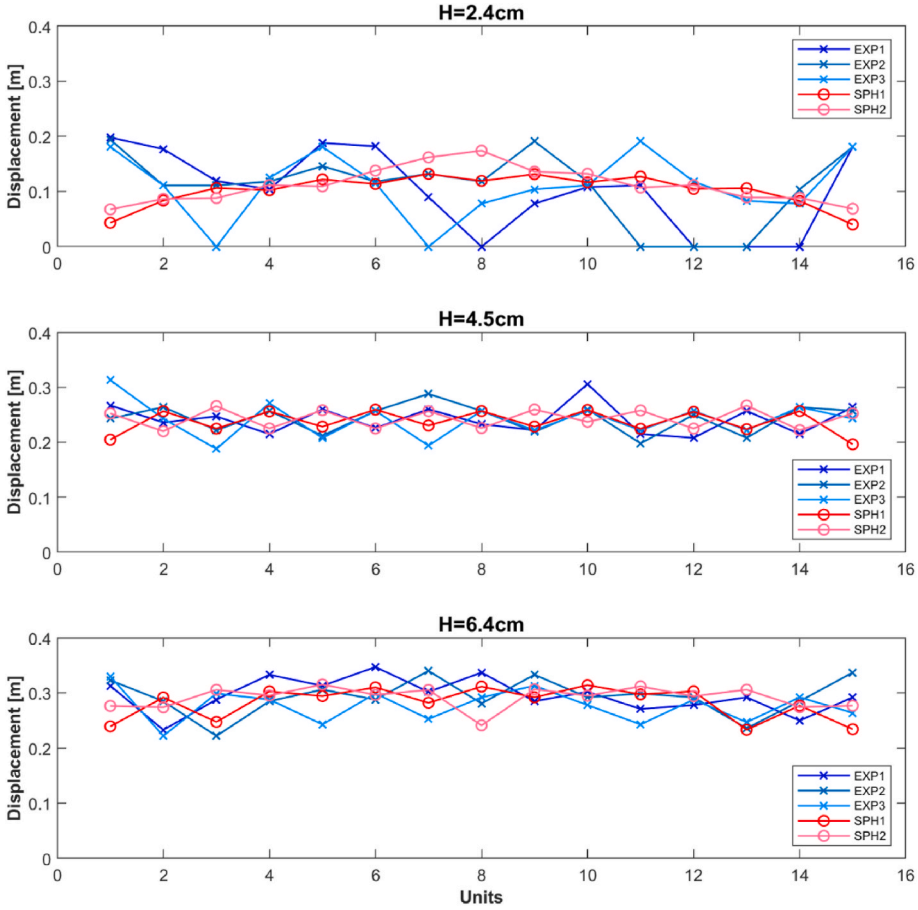

Fig. 12. Experimental and numerical displacements of the 15 Tetrapods during the experimental tests (EXP1, EXP2, EXP3) and numerical simulations (SPH1, SPH2).

Table 3
Experimental and numerical displacement of Tetrapods with PVC mound.

	$H_{WG1} = 2.6$ cm	$H_{WG1} = 4.5$ cm	$H_{WG1} = 6.4$ cm
EXP1	0.102 m	0.242 m	0.296 m
EXP2	0.109 m	0.244 m	0.294 m
EXP3	0.110 m	0.241 m	0.277 m
EXP	*0.107 ± 0.004 m*	*0.242 ± 0.002 m*	*0.289 ± 0.010 m*
SPH1	0.102 m	0.237 m	0.282 m
SPH2	0.111 m	0.243 m	0.292 m
SPH	*0.106 ± 0.006 m*	*0.240 ± 0.004*	*0.287 ± 0.007 m*
ERROR	**0.7%**	**0.8%**	**0.6%**

Table 4
Experimental and numerical damage of Tetrapods with PVC mound. Number of blocks that move more than 7.7 cm are also included in parenthesis.

	$H_{WG1} = 2.6$ cm	$H_{WG1} = 4.5$ cm	$H_{WG1} = 6.4$ cm
EXP1	73% (11)	100% (15)	100% (15)
EXP2	80% (12)	100% (15)	100% (15)
EXP3	87% (13)	100% (15)	100% (15)
SPH1	87% (13)	100% (15)	100% (15)
SPH2	87% (13)	100% (15)	100% (15)

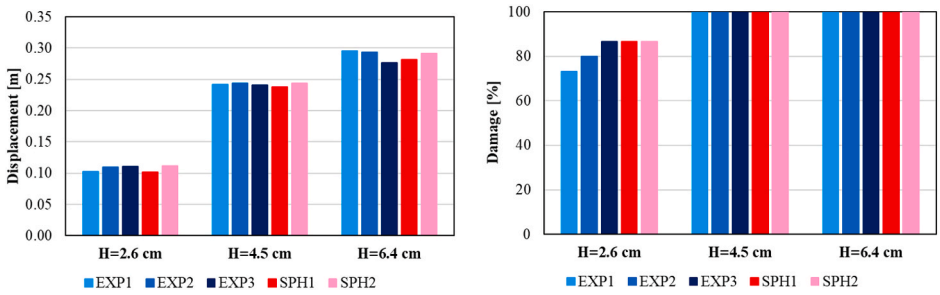

Fig. 13. Bar chart of the experimental and numerical displacement (left) and damage (right) of Tetrapods with PVC mound.

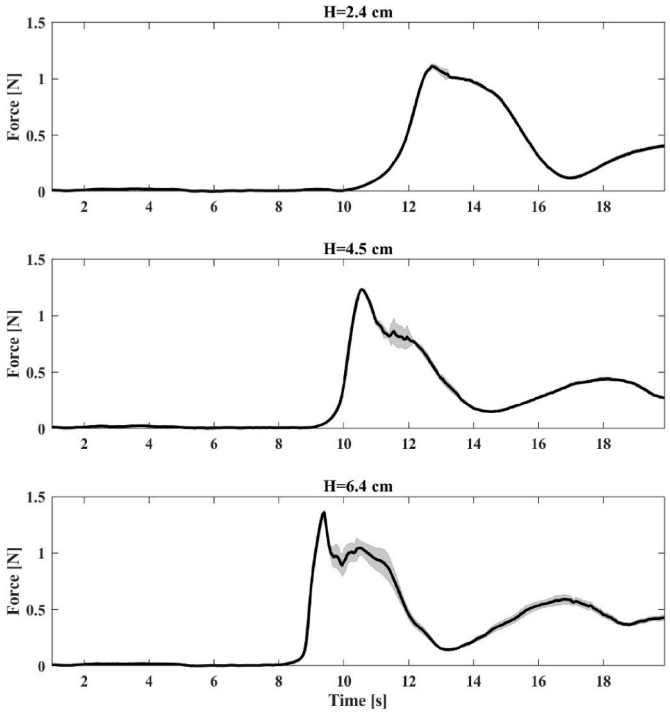

Fig. 14. Time series of the numerical wave force experience by the Tetrapods for the different wave conditions.

second, third and fourth frames and the wave has already passed in the last three ones. Note that this central Tetrapod rotates under the action of wave of $H_{WG1} = 4.5$ cm. The interest here is to observe the smooth pressure field present in all the instants of the figure. Velocity values of the fluid particles are plotted in the right panels of the figure. It is also worth mentioning how mDBC allows the fluid to approach the boundary limit defined by the geometry of the Tetrapod. On the other hand, an irregular particle distribution around the free surface can be observed in some frames of Fig. 15. Despite the enhanced stability and accuracy of the density diffusion term by Fourtakas et al. (2019), two incompressibility conditions corresponding to the invariant density condition and divergence-free velocity condition are not completely resolved. The work of Khayyer et al. (2023) proposed two novel schemes, Velocity-divergence Error Mitigating (VEM) and Volume Conservation Shifting (VCS), which provide more regular and spatially continuous particle distributions around the free surface.

4.6. Convergence and performance analysis

This section includes the convergence analysis that was performed to select the most suitable numerical resolution used to obtain the results presented in the previous section. All previous simulations use the initial interparticle distance of $dp = 0.005$ m following the recommendation $H/dp > 5$, so that 5, 9 and 13 particles discretise the three different solitary wave heights at WG1. As mentioned before, using this resolution, 15 particles were created in the size of a Tetrapod (7.7 cm). A complete convergence study includes now the results of using different initial interparticle distances. In this case, $dp = 9$, 7, 5 and 4 mm are used to discretise the Tetrapod with 8, 11, 15, and 19 particles per size, respectively (Table 5).

Fig. 16 collects the average displacements for the three repetitions of the experiments and for the simulations with different resolutions using only the configuration SPH1. Convergence is achieved since numerical results using $dp = 0.004$ m do not really improve the ones achieved already with $dp = 0.005$ m.

Another important aspect to be considered to evaluate the capability of a numerical tool is the computational performance since it is desirable that simulations are executed at an affordable computational time. Table 6 includes the runtimes of all previous simulations executed on a NVIDIA GeForce RTX 3080Ti GPU with Intel i7-8700K CPU. In order to make a decision about the best numerical resolution, a good balance between accuracy (error values in Table 6) and runtime should be achieved. Both highest resolutions $dp = 0.005$ m and 0.004 m provide errors smaller than 5% while executions take 1.25 days and 3 days, respectively. Therefore, $dp = 0.005$ m is a good compromise with runtimes that can be considered as reasonable.

Whereas the DualSPHysics is executed on the GPU card, the collision detection of the Project Chrono library is executed on single-core CPU. It can be observed how increasing resolution, the total simulation time increases since more interactions and SPH particles need to be solved and because time step is smaller. However, the time dedicated to solve solid interactions is the same (around the 4 h) since the same number of objects (and surfaces) colliding need to be solved by Chrono and this is independent of the SPH resolution. Special care should be paid if the number of blocks increases (or the number of layers of units in the armour layer) since the runtime of the multiphysics library is really dependent on that (Martínez-Estévez et al., 2023).

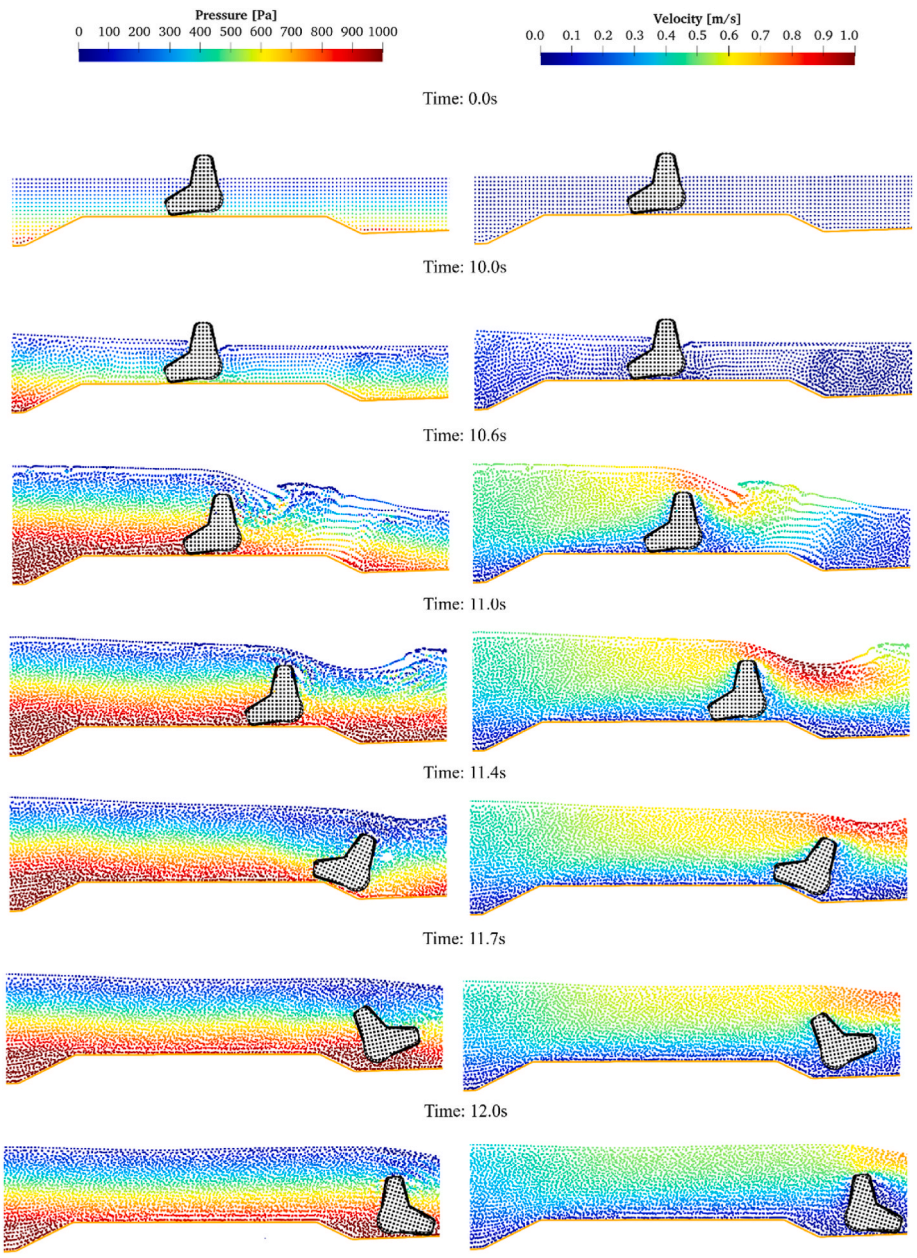

Fig. 15. Different instants of the interaction between solitary wave of $H_{WG1} = 4.5$ cm with the central Tetrapod. Colour of fluid particles correspond to the pressure field (left) and velocity field (right).

Table 5
Number of particles and particles per Tetrapod size (7.7 cm) for different resolutions.

Particle spacing (*dp*)	Number of total particles	Number of floating particles	Particles/ Tetrapod size
0.009 m	3,659,860	2,622 *(15 blocks)*	8
0.007 m	7,036,521	5,655 *(15 blocks)*	11
0.005 m	17,541,570	15,385 *(15 blocks)*	15
0.004 m	32,502,271	29,831 *(15 blocks)*	19

4.7. Effect of the roughness of the mound

The numerical tool was properly validated with specific experiments where the movements of the Tetrapods were carefully obtained and the actual geometry and properties (mass and friction coefficient) of the blocks and the mound were used in the simulations. The experimental campaign was conducted with Tetrapods made of mortar and a mound of PVC. The friction coefficients were 0.65 in the case of mortar-mortar and 0.32 for PVC-mortar. In this section, the roughness of the mound is varied. The aim is to represent mounds of different materials or the effects of material deterioration in time or under cyclic loading, which

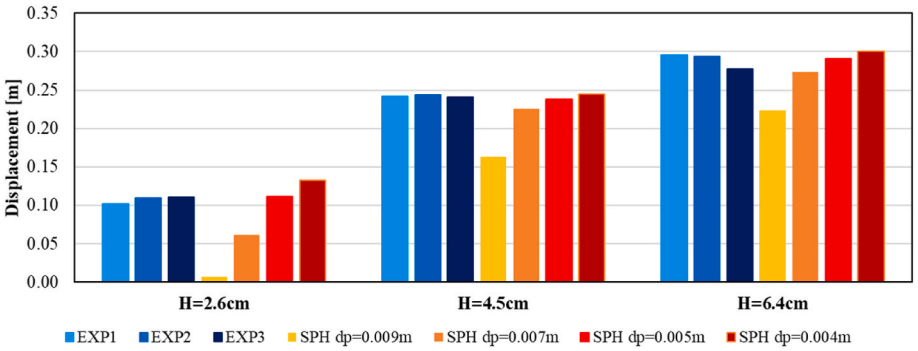

Fig. 16. Bar chart of the experimental and numerical displacement of Tetrapods with PVC mound for the different experimental tests and numerical simulations with different resolutions.

Table 6
Initial particle spacing, number of particles, computational times and error comparing with experimental results using four different resolutions.

Configuration	Particle spacing (dp)	Number of total particles	Runtime	Error SPH1 vs EXP
$H_{WG1} = 2.6$ cm	0.009 m	3,659,860	7.21 h	93.6%
	0.007 m	7,036,521	10.84 h	42.6%
	0.005 m	17,541,570	29.90 h	4.4%
	0.004 m	32,502,271	68.78 h	−2.8%
$H_{WG1} = 4.5$ cm	0.009 m	3,659,860	6.78 h	32.5%
	0.007 m	7,036,521	11.21 h	7.1%
	0.005 m	17,541,570	30.42 h	2.0%
	0.004 m	32,502,271	69.50 h	−1.6%
$H_{WG1} = 6.4$ cm	0.009 m	3,659,860	7.53 h	22.6%
	0.007 m	7,036,521	10.81 h	5.3%
	0.005 m	17,541,570	30.44 h	2.1%
	0.004 m	32,502,271	70.08 h	−4.0%

inevitably modifies the surface properties and hence the shear friction (e.g. Taklas et al., 2022). In particular, the following values of the coefficient of friction between the mound and the Tetrapods have been modelled: 0.10, 0.21, 0.32, 0.43, 0.54, 0.65, 0.76, 0.87 and 0.98.

The average displacement and the damage rate are computed from the results of the simulations that consider different coefficients of friction (COF) and always using $dp = 0.005$ m. Final instants after the solitary wave has passed are depicted in Fig. 17 for the coefficients of friction between Tetrapods and mound equal to 0.10, 0.32, 0.54 and 0.76. It can be observed that the displacement of the units increases with the wave height and decreases with the roughness of the mound, as expected.

All the values of displacements and damage rates are plotted in Fig. 18 for a more exhaustive analysis. As expected, the higher the wave height, the higher the displacement for both settings. The minimum friction coefficient simulated here (0.10) provides the highest displacements, which are 0.32 m with the wave of $H_{WG1} = 2.6$ cm, 0.37 m with the wave of $H_{WG1} = 4.5$ cm and 0.68 m with the wave of $H_{WG1} = 6.4$ cm. Then, the displacement decreases with the coefficient of friction. In fact, Tetrapods do not move at all for friction coefficients higher than 0.32, 0.54, respectively for the two first solitary waves, and with $H_{WG1} = 6.4$ cm displacements are less than 0.07 m for coefficients of friction higher than 0.65.

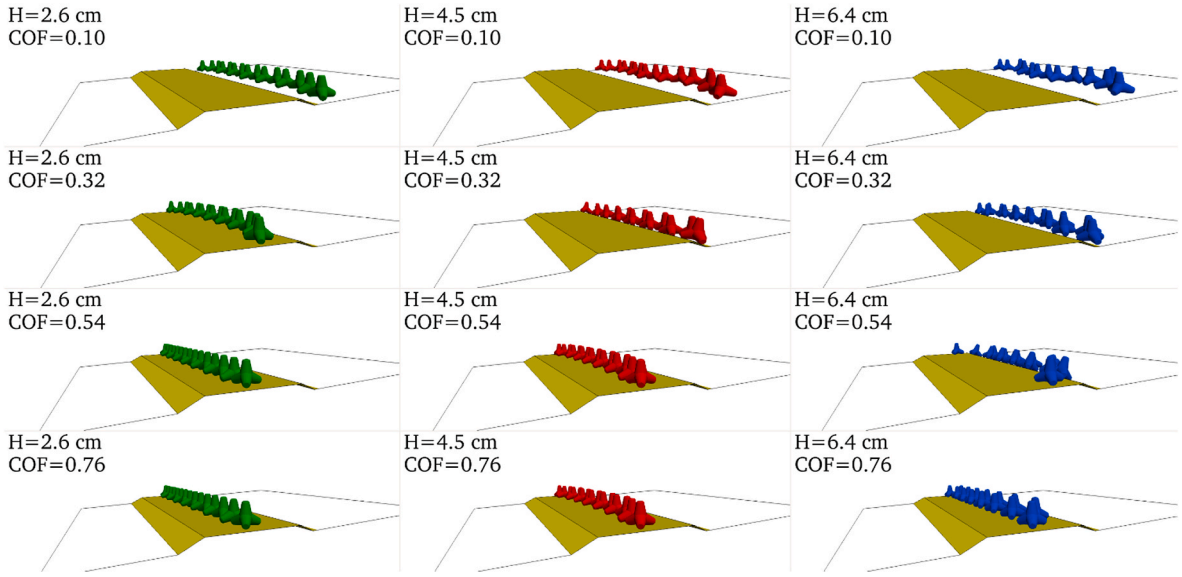

Fig. 17. Final situation of Tetrapods over mound with different roughness.

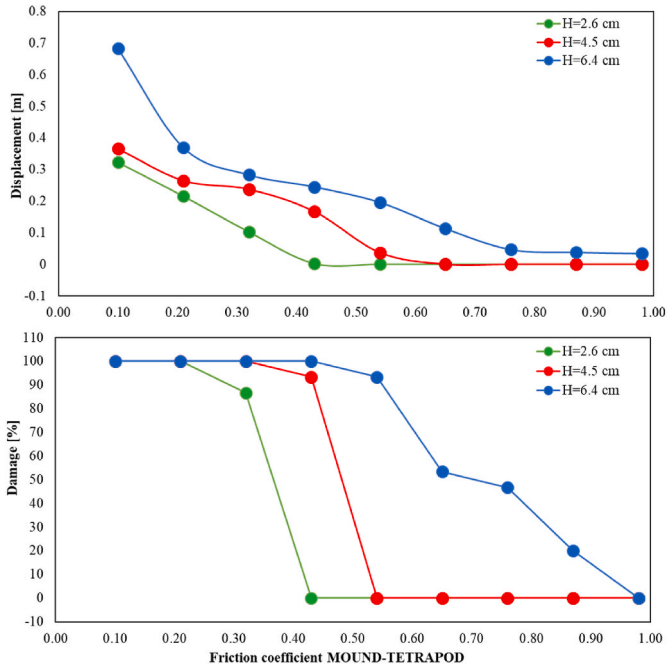

Fig. 18. Displacements (top) and damage rates (bottom) for different friction coefficients between Tetrapods and mound.

5. Conclusions

In the present work, the open-source DualSPHysics solver is applied to model the performance and behaviour of Tetrapod units under solitary wave attack. The model, based on the Smoothed Particle Hydrodynamics (SPH) method, is coupled with the multiphysics library Project Chrono, to solve the interaction between Tetrapods units and the mound of the breakwater. The meshless nature of SPH allows modelling rapidly moving complex boundaries, fluid-driven bodies and complex interfaces, going beyond the limitations of mesh-based methods. The coupled DualSPHysics-Chrono model is validated against experimental data of solitary waves hitting single layers of Tetrapod units placed on a submerged PVC mound. The model was proven to reproduce the unit displacement and damage ratio measured experimentally. Then, the model is extended to study the stability while varying the friction of the foundation mound and studying the variation of the armour layer response.

In order to minimise the discrepancies observed between experiments and our numerical results, several strategies should be adopted in the forthcoming investigations regarding the SPH method and the contact models between solids. More sophisticated approaches should be further investigated and applied here such as delta-SPH (Antuono et al., 2012) and its more recent variant deltaplus-SPH (Sun et al., 2017), Riemann solvers (Vila, 1999), Incompressible SPH (Lind et al., 2012; Khayyer et al., 2017). The effect of turbulence could be also considered in a future work by using the laminar viscosity implementation together with the Sub-Particle Scale (SPS) turbulence model. The SPS model was first described by Gotoh et al. (2001) to represent the effects of turbulence in their Moving Particle Semi-implicit (MPS) model and later introduced into weakly compressible SPH by Dalrymple and Rogers (2006). Regarding the contact model, it will be worth to compare the implementation in Project Chrono, where collision detection is solved in terms of geometries, against the previous implementation of DEM available in DualSPHysics presented in Canelas et al. (2016), where contact forces of the bodies are solved based on particle interactions. Thus, refining the SPH resolution, the accuracy of the numerical results may be improved, but the computational resources would be far more demanding than using Chrono.

Further investigation to provide a more in-depth systematic analysis of wave interactions with armour units of breakwaters should include the modelling of Tetrapods interlocking. First, similar validations as the ones conducted in Canelas et al. (2016), Canelas et al. (2017) and Sarfaraz and Pak (2018) using DEM should be carried out now with Project Chrono. In this way, interaction between cubes will be first validated without waves. Secondly, a new experimental campaign would have to include collisions among Tetrapods as well, considering, for example, a two-layer breakwater configuration.

The outcomes of the presented research demonstrate that SPH-based codes are unique and versatile tools to study the stability of armour breakwaters. The work carried out, in fact, can be extended to study the performance of armour units having different nominal diameter, density, shape or interlocking properties, aiding the design of coastal protections. Thus, meshless methods represent feasible alternatives or complementary tools to more expensive and time-consuming experimental campaigns to characterise stability and damage evolution of armour layers and revetments.

Declaration of competing interest

The authors declare that they have no known competing financial interests or personal relationships that could have appeared to influence the work reported in this paper.

Data availability

Data will be made available on request.

Acknowledgements

Funding for open access charge: Universidade de Vigo/CISUG. This work was supported by the projects PID2020-113245RB-I00 and TED2021-129479A-I00 financed by MCIN/AEI/10.13039/501100011033 and by the project ED431C 2021/44 “Programa de Consolidación e Estructuración de Unidades de Investigación Competitivas” financed by Xunta de Galicia, Consellería de Cultura, Educación e Universidade. This study forms part of the Marine Science programme (ThinkInAzul) supported by Ministerio de Ciencia e Innovación and Xunta de Galicia with funding from European Union NextGenerationEU (PRTR-C17.I1) and European Maritime and Fisheries Fund. I. Martínez-Estévez acknowledges funding from Xunta de Galicia under “Programa de axudas á etapa predoutoral da Consellería de Cultura, Educación e Universidades da Xunta de Galicia” (ED481A-2021/337). Dr. Corrado Altomare acknowledges funding from Spanish government and the European Social Found (ESF) under the programme ‘Ramón y Cajal 2020’ (RYC2020-030197-I/AEI/10.13039/501100011033).

Appendix A

The following tables include the individual displacements of the 15 Tetrapods during the three repetitions of the experiments (EXP1, EXP2, EXP3) and for the two numerical configurations (SPH1, SPH2). Average and standard deviation (*STD*) values are also computed. Each table refers to each of the three solitary wave heights.

Table A1
Displacements of the Tetrapods during the experiments and the numerical simulations for $H_{WG1} = 2.6$ cm (all units are in meters).

Block No.	EXP1	EXP2	EXP3	SPH1	SPH2
1	0.198	0.194	0.181	0.043	0.068
2	0.177	0.111	0.111	0.084	0.087
3	0.119	0.111	0.000	0.106	0.088
4	0.104	0.118	0.125	0.102	0.112
5	0.188	0.146	0.181	0.122	0.109
6	0.182	0.118	0.115	0.114	0.138
7	0.090	0.132	0.000	0.132	0.162
8	0.000	0.118	0.078	0.119	0.174
9	0.078	0.191	0.104	0.131	0.136
10	0.108	0.118	0.111	0.117	0.132
11	0.111	0.000	0.191	0.127	0.107
12	0.000	0.000	0.118	0.105	0.112
13	0.000	0.000	0.083	0.106	0.089
14	0.000	0.104	0.078	0.083	0.088
15	0.181	0.181	0.181	0.040	0.069
AVERAGE	**0.102**	**0.109**	**0.110**	**0.102**	**0.111**
STD	***0.074***	***0.064***	***0.059***	***0.029***	***0.032***

Table A2
Displacements of the Tetrapods during the experiments and the numerical simulations for $H_{WG1} = 4.5$ cm (all units are in meters).

Block No.	EXP1	EXP2	EXP3	SPH1	SPH2
1	0.267	0.243	0.313	0.205	0.253
2	0.236	0.264	0.243	0.257	0.220
3	0.247	0.222	0.188	0.225	0.266
4	0.215	0.257	0.271	0.256	0.225
5	0.260	0.212	0.208	0.228	0.258
6	0.226	0.257	0.257	0.259	0.225
7	0.260	0.288	0.194	0.231	0.257
8	0.233	0.257	0.257	0.257	0.226
9	0.222	0.219	0.222	0.229	0.260
10	0.306	0.260	0.257	0.259	0.237
11	0.215	0.198	0.222	0.225	0.258
12	0.208	0.250	0.257	0.255	0.225
13	0.257	0.208	0.222	0.224	0.267
14	0.215	0.264	0.264	0.257	0.222
15	0.264	0.257	0.243	0.196	0.253
AVERAGE	**0.242**	**0.244**	**0.241**	**0.237**	**0.243**
STD	***0.027***	***0.026***	***0.033***	***0.021***	***0.018***

Table A3
Displacements of the Tetrapods during the experiments and the numerical simulations for $H_{WG1} = 6.4$ cm (all units are in meters).

Block No.	EXP1	EXP2	EXP3	SPH1	SPH2
1	0.313	0.323	0.330	0.239	0.277
2	0.233	0.285	0.222	0.292	0.274
3	0.288	0.222	0.299	0.248	0.306
4	0.333	0.285	0.288	0.303	0.296
5	0.313	0.306	0.243	0.294	0.315
6	0.347	0.288	0.299	0.310	0.297
7	0.302	0.340	0.253	0.282	0.306
8	0.337	0.281	0.292	0.312	0.241
9	0.285	0.333	0.313	0.292	0.307
10	0.302	0.292	0.278	0.314	0.295
11	0.271	0.299	0.243	0.297	0.312
12	0.278	0.292	0.288	0.303	0.294
13	0.292	0.236	0.247	0.233	0.306
14	0.250	0.285	0.292	0.277	0.274
15	0.292	0.337	0.264	0.234	0.277
AVERAGE	**0.296**	**0.294**	**0.277**	**0.282**	**0.292**
STD	***0.031***	***0.033***	***0.030***	***0.029***	***0.020***

References

Altomare, C., Crespo, A.J.C., Rogers, B.D., Domínguez, J.M., Gironella, X., Gómez-Gesteira, M., 2014. Numerical modelling of armour block sea breakwater with Smoothed Particle Hydrodynamics. Comput. Struct. 130, 34–45.

Altomare, C., Crespo, A.J.C., Domínguez, J.M., Gómez-Gesteira, M., Suzuki, T., Verwaest, T., 2015a. Applicability of Smoothed Particle Hydrodynamics for estimation of sea wave impact on coastal structures. Coast. Eng. 96, 1–12.

Altomare, C., Domínguez, J.M., Crespo, A.J.C., Suzuki, T., Caceres, I., Gómez-Gesteira, M., 2015b. Hybridization of the wave propagation model SWASH and the meshfree particle method SPH for real coastal applications. Coast Eng. J. 57 (4), 1550024.

Altomare, C., Domínguez, J.M., Crespo, A.J.C., González-Cao, J., Suzuki, T., Gómez-Gesteira, M., Troch, P., 2017. Long-crested wave generation and absorption for SPH-based DualSPHysics model. Coast. Eng. 127, 37–54.

Altomare, C., Tagliafierro, B., Domínguez, J.M., Suzuki, T., Viccione, G., 2018. Improved relaxation zone method in SPH-based model for coastal engineering applications. Appl. Ocean Res. 81, 15–33. https://doi.org/10.1016/j.apor.2018.09.013.

Altomare, C., Tafuni, A., Domínguez, J.M., Crespo, A.J.C., Gironella, X., Sospedra, J., 2020. SPH simulations of real sea waves impacting a large-scale structure. J. Mar. Sci. Eng. 8, 826. https://doi.org/10.3390/jmse8100826.

Altomare, C., Gironella, X., Crespo, A.J.C., 2021. Simulation of random wave overtopping by a WCSPH model. Appl. Ocean Res. 116, 102888 https://doi.org/10.1016/j.apor.2021.102888.

Antuono, M., Colagrossi, A., Marrone, S., 2012. Numerical diffusive terms in weakly-compressible SPH schemes. Comput. Phys. Commun. 183 (12), 2570–2580.

Asai, M., Li, Yi, Chandra, B., Takase, S., 2021. Fluid–rigid-body interaction simulations and validations using a coupled stabilized ISPH–DEM incorporated with the energy-tracking impulse method for multiple-body contacts. Comput. Methods Appl. Mech. Eng. 377, 113681 https://doi.org/10.1016/j.cma.2021.113681.

Bouscasse, B., Colagrossi, A., Marrone, S., Antuono, M., 2013. Nonlinear water wave interaction with floating bodies in SPH. J. Fluid Struct. 42, 112–129.

Campos, Á., Molina-Sánchez, R., Castillo, C., 2020. Damage in rubble mound breakwaters. Part II: review of the definition, parameterization, and measurement of damage. J. Mar. Sci. Eng. 8, 306. https://doi.org/10.3390/jmse8050306.

Canelas, R.B., Domínguez, J.M., Crespo, A.J.C., Gómez-Gesteira, M., Ferreira, R.M.L., 2015. A Smooth Particle Hydrodynamics discretization for the modelling of free surface flows and rigid body dynamics. Int. J. Numer. Methods Fluid. 78, 581–593.

Canelas, R.B., Crespo, A.J.C., Domínguez, J.M., Ferreira, R.M.L., Gómez-Gesteira, M., 2016. SPH–DCDEM model for arbitrary geometries in free surface solid–fluid flows. Comput. Phys. Commun. 202, 131–140. https://doi.org/10.1016/j.cpc.2016.01.006.

Canelas, R.B., Domínguez, J.M., Crespo, A.J.C., Gómez-Gesteira, M., 2017. Resolved simulation of a granular-fuid fow with a coupled SPH-DCDEM model. J. Hydraul. Eng. 143, 06017012 https://doi.org/10.1061/(ASCE)HY.1943-7900.0001331.

Canelas, R.B., Crespo, A.J.C., Brito, M., Domínguez, J.M., García-Feal, O., 2018. Extending DualSPHysics with a differential variational inequality: modeling fluid-mechanism interaction. Appl. Ocean Res. 76, 88–97.

Celli, D., Pasquali, D., Fischione, P., Di Nucci, C., Di Risio, M., 2021. Wave-induced dynamic pressure under rubble mound breakwaters with submerged berm: an experimental and numerical study. Coast. Eng. 170, 104014 https://doi.org/10.1016/j.coastaleng.2021.104014.

Chandar, D.D., 2019. On overset interpolation strategies and conservation on unstructured grids in OpenFOAM. Comput. Phys. Commun. 239, 72–83.

Crespo, A.J.C., Gómez-Gesteira, M., Dalrymple, R.A., 2007. Boundary conditions generated by dynamic particles in SPH methods. Comput. Mater. Continua (CMC): Comput. Mater. Continua (CMC) 5 (3), 173–184.

Dalrymple, R.A., Rogers, B.D., 2006. Numerical modeling of water waves with the SPH method. Coast. Eng. 53, 141–147.

Danel, P., Greslou, L., 1962. The “Tetrapod”. Coastal Engineering Proceedings 1 (8), 27. https://doi.org/10.9753/icce.v8.27.

Dentale, F., Reale, F., Di Leo, A., Publiese Carratelli, E., 2018. A CFD approach to rubble mound breakwater design. Int. J. Nav. Archit. Ocean Eng. 10 (5), 644–650. https://doi.org/10.1016/j.ijnaoe.2017.10.011.

Domínguez, J.M., Crespo, A.J.C., Hall, M., Altomare, C., Wu, M., Stratigaki, V., Troch, P., Cappietti, L., Gómez-Gesteira, M., 2019a. SPH simulation of floating structures with moorings. Coast. Eng. 153, 103560 https://doi.org/10.1016/j.coastaleng.2019.103560.

Domínguez, J.M., Altomare, C., González-Cao, J., Lomonaco, P., 2019b. Towards a more complete tool for coastal engineering: solitary wave generation, propagation and breaking in an SPH-based model. Coast Eng. J. 61, 15–40. https://doi.org/10.1080/21664250.2018.1560682.

Domínguez, J.M., Fourtakas, G., Altomare, C., Canelas, R.B., Tafuni, A., García-Feal, O., Martínez-Estévez, I., Mokos, A., Vacondio, R., Crespo, A.J.C., Rogers, B.D., Stansby, P.K., Gómez-Gesteira, M., 2022. DualSPHysics: from fluid dynamics to multiphysics problems. Comput. Part. Mech. 9 (5), 867–895. https://doi.org/10.1007/s40571-021-00404-2.

English, A., Domínguez, J.M., Vacondio, R., Crespo, A.J.C., Stansby, P.K., Lind, S.J., Chiapponi, L., Gómez-Gesteira, M., 2022. Modified dynamic boundary conditions (mDBC) for general purpose smoothed particle hydrodynamics (SPH): application to tank sloshing, dam break and fish pass problems. Comput. Part. Mech. 9 (5), 911–925. https://doi.org/10.1007/s40571-021-00403-3.

Esteban, M., Jayaratne, R., Mikami, T., Morikubo, I., Shibayama, T., Thao, N.D., Ohira, K., Ohtani, A., Mizuno, Y., Kinoshita, M., Matsuba, S., 2014. Stability of breakwater armor units against tsunami attacks. J. Waterw. Port, Coast. Ocean Eng. 140 (2), 188–198.

Fourtakas, G., Domínguez, J.M., Vacondio, R., Rogers, B.D., 2019. Local uniform stencil (LUST) boundary condition for arbitrary 3-D boundaries in parallel smoothed particle hydrodynamics (SPH) models. Comput. Fluids 190, 346–361. https://doi.org/10.1016/j.compfluid.2019.06.009.

Goring, D., Raichlen, F., 1980. The generation of long waves in the laboratory. Coastal Engineering Proceedings 1 (17), 46. https://doi.org/10.9753/icce.v17.46.

Gotoh, H., Shibahara, T., Sakai, T., 2001. Sub-particle-scale turbulence model for the MPS method - Lagrangian flow model for hydraulic engineering. Comput. Fluid Dynam. J. 9 (4), 339–347.

Gotoh, H., Harada, E., Ikari, H., Ooe, K., Yasuoka, T., 2010. Numerical simulation of deformation process of armor blocks by DEM-MPS coupling model. J. JSCE, Ser B 66 (3), 258–267.

Gotoh, H., Khayyer, A., 2018. On the state-of-the-art of particle methods for coastal and ocean engineering. Coast Eng. J. 60, 79–103.

Güler, H.G., Baykal, C., Arikawa, T., Yalçıner, A.C., 2018. Numerical assessment of tsunami attack on a rubble mound breakwater using OpenFOAM (R). Appl. Ocean Res. 72, 76–91. https://doi.org/10.1016/j.apor.2018.01.005.

Hagemeier, T., Thévenin, D., Richter, T., 2021. Settling of spherical particles in the transitional regime. Int. J. Multiphas. Flow 138, 103589. https://doi.org/10.1016/j.ijmultiphaseflow.2021.103589.

Hanzawa, M., Sato, H., Takahashi, S., Shimosako, K., Takayama, T., Tanimoto, K., 1996. New stability formula for wave-dissipating concrete blocks covering horizontally composite breakwaters. Coastal Engineering Proceedings 1 (25). https://doi.org/10.9753/icce.v25.%25p.

Hanzawa, M., Matsumoto, A., Tanaka, H., 2012. Stability of wave-dissipating concrete blocks of detached breakwaters against tsunami. Coastal Engineering Proceedings 1 (33), 24. https://doi.org/10.9753/icce.v33.structures.24 structures.

Harada, E., Gotoh, H., Tsuruta, N., 2011. Numerical simulation for sedimentation process of blocks on a sea bed by high-resolution multi-phase model. Coast Eng. J. 53 (4), 343–364.

Hudson, R.Y., 1959. Laboratory investigation of rubble-mound breakwater. J. Waterw. Harb. Div. 85 (WW3), 93–121.

Ikari, H., Gotoh, H., 2022. Fully implicit discrete element method for granular column collapse. Comput. Part. Mech. 1–11.

Khayyer, A., Gotoh, H., Shimizu, Y., 2017. Comparative study on accuracy and conservation properties of two particle regularization schemes and proposal of an optimized particle shifting scheme in ISPH context. J. Comput. Phys. 332, 236–256. https://doi.org/10.1016/j.jcp.2016.12.005.

Khayyer, A., Shimizu, Y., Gotoh, T., Gotoh, H., 2023. Enhanced resolution of the continuity equation in explicit weakly compressible SPH simulations of incompressible free-surface fluid flows. Appl. Math. Model. 116, 84–121.

Koley, S., Panduranga, K., Almashan, N., Neelamani, S., Al-Ragum, A., 2020. Numerical and experimental modeling of water wave interaction with rubble mound offshore porous breakwaters. Ocean Eng. 218, 108218 https://doi.org/10.1016/j.oceaneng.2020.108218.

Kortenhaus, A., Oumeraci, H., 1998. Classification of wave loading on monolithic coastal structures. Proc. Coast. Eng. Conf. 1, 867–880.

Leimkuhler, B.J., Matthews, C., 2015. Introduction. In: Molecular Dynamics: with Deterministic and Stochastic Numerical Methods, pp. 1–51.

Lind, S., Xu, R., Stansby, P., Rogers, B., 2012. Incompressible smoothed particle hydrodynamics for free-surface flows: a generalised diffusion-based algorithm for stability and validations for impulsive flows and propagating waves. J. Comput. Phys. 231 (4), 1499–1523. https://doi.org/10.1016/j.jcp.2011.10.027.

Liu, M.B., Liu, G.R., 2006. Restoring particle consistency in smoothed particle hydrodynamics. Appl. Numer. Math. 56, 19–36.

Macía, F., González, L.M., Cercos-Pita, J.L., Souto-Iglesias, A., 2012. A boundary integral SPH formulation. Consistency and applications to ISPH and WCSPH. Prog. Theor. Phys. 128 (3) https://doi.org/10.1143/PTP.128.439.

Manenti, S., Wang, D., Domínguez, J.M., Li, S., Amicarelli, A., Albano, R., 2019. SPH modeling of water-related natural hazards. Water 11 (9), 1875. https://doi.org/10.3390/w11091875.

Mares-Nasarre, P., Molines, J., Gómez-Martín, M.E., Medina, J.R., 2022. Hydraulic stability of cube-armored mound breakwaters in depth-limited breaking wave conditions. Ocean Eng. 259, 111845 https://doi.org/10.1016/j.oceaneng.2022.111845. ISSN 0029-8018.

Marrone, S., Antuono, M., Colagrossi, A., Colicchio, G., Le Touzé, D., Graziani, G., 2011. δ-SPH model for simulating violent impact flows. Comput. Methods Appl. Mech. Eng. 200 (13–16), 1526–1542.

Martínez-Estévez, I., Domínguez, J.M., Tagliafierro, B., Canelas, R.B., García-Feal, O., Crespo, A.J.C., Gómez-Gesteira, M., 2023. Coupling of an SPH-based solver with a multiphysics library. Comput. Phys. Commun. 283, 108581 https://doi.org/10.1016/j.cpc.2022.108581.

Maruyama, S., Mitsui, J., Matsumoto, A., Hanzawa, M., 2014. Armor damage on harbor-side rubble mound of composite breakwaters against water jet caused by impinging bore-like tsunami. Coastal Engineering Proceedings 1 (34), 35. https://doi.org/10.9753/icce.v34.structures.35 structures.

Mitsui, J., Matsumoto, A., Hanzawa, M., Nadaoka, K., 2014. Stability of armor units convering rubble mound of composite breakwaters against a steady overflow of tsunami. Coastal Engineering Proceedings 1 (34). https://doi.org/10.9753/icce.v34.structures.34.

Mitsui, J., Matsumoto, A., Hanzawa, M., Nadaoka, K., 2016. Estimation method of armor stability against tsunami overtopping caisson breakwater based on overflow depth. Coast Eng. J. 58 (4), 1640019.

Molteni, D., Colagrossi, A., 2009. A simple procedure to improve the pressure evaluation in hydrodynamic context using the SPH. Comput. Phys. Commun. 180, 861–872. https://doi.org/10.1016/j.cpc.2008.12.004.

Monaghan, J.J., 1992. Smoothed particle hydrodynamics. Annu. Rev. Astron. Astrophys. 30, 543–574.
Monaghan, J.J., Cas, R.A.F., Kos, A.M., Hallworth, M., 1999. Gravity currents descending a ramp in a stratified tank. J. Fluid Mech. 379, 39–70.
Oger, G., Vergnaud, A., Bouscasse, B., Ohana, J., Abu Zarim, M., De Leffe, M., Bannier, A., Chiron, L., Jus, Y., Garnier, M., Halbout, S., Le Touzé, D., 2020. Simulations of helicopter ditching using smoothed particle hydrodynamics. J. Hydrodyn. 32, 653–663.
Omidvar, P., Stansby, P.K., Rogers, B.D., 2013. SPH for 3D floating bodies using variable mass particle distributions. Int. J. Numer. Methods Fluid. 72, 427–452.
Parshikov, A.N., Medin, S.A., Loukashenko, I.I., Milekhin, V.A., 2000. Improvements in SPH method by means of interparticle contact algorithm and analysis of perforation tests at moderate projectile velocities. Int. J. Impact Eng. 24, 779–796. https://doi.org/10.1016/S0734-743X(99)00168-2.
Rogers, B.D., Dalrymple, R.A., Stansby, P.K., 2010. Simulation of caisson breakwater movement using 2-D SPH. J. Hydraul. Res. 48, 135–141. https://doi.org/10.1080/00221686.2010.9641254.
Rota-Roselli, R.A., Vernengo, G., Altomare, C., Brizzolara, S., Bonfiglio, L., Guercio, R., 2018. Ensuring numerical stability of wave propagation by tuning model parameters using genetic algorithms and response surface methods. Environ. Model. Software 103, 62–73.
Sande, J., Peña, E., Maciñeira, E., 2018. Stability of breakwater roundhead protected with a Cubipod single-layer armor. Appl. Ocean Res. 79, 36–48.
Safari, I., Mouazé, D., Ropert, F., Haquin, S., Ezersky, A., 2018. Hydraulic stability and wave overtopping of Starbloc® armored mound breakwaters. Ocean Eng. 151, 268–275. https://doi.org/10.1016/j.oceaneng.2017.12.061. ISSN 0029-8018.
Sarfaraz, M., Pak, A., 2018. Numerical investigation of the stability of armour units in low-crested breakwaters using combined SPH–Polyhedral DEM method. J. Fluid Struct. 81, 14–35. https://doi.org/10.1016/j.jfluidstructs.2018.04.016.
Shadloo, M.S., Oger, G., Le Touzé, D., 2016. Smoothed particle hydrodynamics method for fluid flows, towards industrial applications: motivations, current state, and challenges. Comput. Fluids 136, 11–34. https://doi.org/10.1016/j.compfluid.2016.05.029.
St-Germain, P., Nistor, I., Townsend, R., Shibayama, T., 2014. Smoothed-Particle Hydrodynamics numerical modeling of structures impacted by tsunami bores. J. Waterw. Port, Coast. Ocean Eng. 140, 66–81.
Sun, P., Colagrossi, A., Marrone, S., Zhang, A., 2017. The delta-plus-SPH model: simple procedures for a further improvement of the SPH scheme. Comput. Methods Appl. Mech. Eng. 315, 25–49.
Sunday, C., Murdoch, N., Tardivel, S., Schwartz, S.R., Michel, P., 2020. Validating n-body code Chrono for granular DEM simulations in reduced-gravity environments. Mon. Not. Roy. Astron. Soc. 498 (1), 1062–1079.
Suzuki, T., García-Feal, O., Domínguez, J.M., Altomare, C., 2022. Simulation of 3D overtopping flow–object–structure interaction with a calibration-based wave generation method with DualSPHysics and SWASH. Comput. Part. Mech. 9 (5), 1003–1015. https://doi.org/10.1007/s40571-022-00468-8.
Taklas, M., Leblouba, M., Barakat, S., Fageeri, A., Mohamad, F., 2022. Concrete-to-concrete shear friction behavior under cyclic loading: experimental investigation. Sci. Rep. 12, 945. https://doi.org/10.1038/s41598-022-13530-5.
Tasora, A., Serban, R., Mazhar, H., Pazouki, A., Melanz, D., Fleis-chmann, J., Taylor, M., Sugiyama, H., Negrut, D., 2016. In: Kozubek, T. (Ed.), Chrono: an Open Source Multi-Physics Dynamics Engine. Springer, pp. 19–49.
Tsuruta, N., Gotoh, H., Suzuki, K., Ikari, H., Shimosako, K., 2019. Development of PARISPHERE as the particle-based numerical wave flume for coastal engineering problems. Coast Eng. J. 61 (1), 41–62.
Vacondio, R., Altomare, C., De Leffe, M., Hu, X., Le Touzé, D., Lind, S., Marongiu, J.-C., Marrone, S., Rogers, B.D., Souto-Iglesias, A., 2020. Grand challenges for smoothed particle hydrodynamics numerical schemes. Comput. Part. Mech. https://doi.org/10.1007/s40571-020-00354-1.
Van der Meer, J.W., 1988. Stability of cubes, tetrapods and accropode. Proc. of Conf. Breakwaters ' 88, 59–68.
Verbrugghe, T., Domínguez, J.M., Altomare, C., Tafuni, A., Vacondio, R., Troch, P., Kortenhaus, A., 2019. Non-linear wave generation and absorption using open boundaries within DualSPHysics. Comput. Phys. Commun. 240, 46–59. https://doi.org/10.1016/j.cpc.2019.02.003.
Vila, J.P., 1999. On particle weighted methods and smooth particle hydrodynamics. Math. Model Methods Appl. Sci. 9 (2), 161–209. https://doi.org/10.1142/S0218202599000117.
Violeau, D., Rogers, B.D., 2016. Smoothed particle hydrodynamics (SPH) for free-surface flows: past, present and future. J. Hydraul. Res. 54 (1), 1–26.
Wendland, H., 1995. Piecewise polynomial, positive definite and compactly supported radial functions of minimal degree. Adv. Comput. Math. 4 (1), 389–396.
Windt, C., Davidson, J., Chandar, D.D., Faedo, N., Ringwood, J.V., 2020. Evaluation of the overset grid method for control studies of wave energy converters in OpenFOAM numerical wave tanks. J. Ocean Eng. Mar. Ener. 6 (1), 55–70.
Yamamoto, T., Yasuda, T., Oguma, K., Matsushita, H., 2022. Numerical simulation of scattering process of armour blocks on additional rubble mound behind breakwater during tsunami overflow using SPH method. Comput. Part. Mech. 9 (5), 953–968. https://doi.org/10.1007/s40571-021-00429-7.
Yuksel, Y., van Gent, M.R.A., Cevik, E., Kaya, A.H., Ari Guner, H.A., Yuksel, Z.T., Gumuscu, I., 2022. Stability of high density cube armoured breakwaters. Ocean Eng. 253 (111317) https://doi.org/10.1016/j.oceaneng.2022.111317. ISSN 0029-8018.
Zhang, F., Crespo, A.J.C., Altomare, C., Domínguez, J.M., Marzeddu, A., Shang, S., Gómez-Gesteira, M., 2018. DualSPHysics: a numerical tool to simulate real breakwaters. J. Hydrodyn. 30 (1), 99–105.
Zijlema, M., Stelling, G., Smit, P., 2011. SWASH: an operational public domain code for simulating wave fields and rapidly varied flows in coastal waters. Coast. Eng. 58, 992–1012. https://doi.org/10.1016/j.coastaleng.2011.05.015.